

# Coupled $f(R)$ Gravity with Neutrinos: A Path to Alleviating Hubble and $S_8$ Tensions.

Muhammad Yarahmadi<sup>1\*</sup>

Department of Physics, Lorestan University, Khorramabad, Iran

(Dated: July 29, 2025)

We investigate the Hubble constant ( $H_0$ ) and  $S_8$  tensions within the framework of perturbed  $f(R)$  gravity models, both with and without neutrino coupling. By analyzing a comprehensive set of cosmological data, including cosmic microwave background (CMB), baryon acoustic oscillations (BAO), cosmic chronometers (CC), Pantheon supernovae, and lensing, we assess the capability of these models to mitigate discrepancies between early- and late-time measurements. The perturbed  $f(R)$  model without neutrino coupling demonstrates moderate improvements in inferred  $H_0$  values, with tensions ranging from  $0.61\sigma$  to  $1.51\sigma$  relative to Planck 2018 and from  $1.10\sigma$  to  $1.44\sigma$  relative to R22. However, the coupled model incorporating neutrino interactions exhibits greater potential to alleviate the Hubble tension, reducing the discrepancy with Planck 2018 to  $0.74\sigma$  and with R22 to  $0.95\sigma$ . Similarly, the coupled model improves consistency in the  $S_8$  parameter, reducing the tension with Planck to  $1.13\sigma$  and lowering tensions with KiDS-1000 and DES-Y3 to  $0.70\sigma$  and  $0.23\sigma$ , respectively. These results highlight the enhanced performance of the neutrino-coupled perturbed  $f(R)$  model in addressing cosmological tensions. While not resolving all discrepancies, the improved agreement with late-time measurements underscores the potential of modified gravity and neutrino interactions to account for deviations in cosmological observations.

PACS numbers:

## I. INTRODUCTION

The Hubble constant ( $H_0$ ) represents the current expansion rate of the Universe and remains one of the most contentious parameters in modern cosmology due to the persistent discrepancy between measurements from early- and late-Universe probes. The two most widely cited methods for determining  $H_0$  are based on observations of the cosmic microwave background (CMB) and Type Ia supernovae (SNe Ia).

The first approach relies on CMB observations, which provide a precise estimate of the Hubble constant by analyzing the angular size of the acoustic peaks in the CMB power spectrum. The Planck collaboration, using seven years of data, reported the most recent estimate in 2018 as  $H_0 = 67.4 \pm 0.5 \text{ km s}^{-1}\text{Mpc}^{-1}$  [3]. This value is consistent with predictions from the standard  $\Lambda$ CDM model but is in significant tension with measurements from late-Universe probes.

In contrast, the second approach, employed by the SH0ES (Supernovae H0 for the Equation of State) collaboration, is based on the Cepheid-calibrated distance ladder using Type Ia supernovae data from the Hubble Space Telescope (HST). The most recent SH0ES result reports  $H_0 = 74.03 \pm 1.42 \text{ km s}^{-1}\text{Mpc}^{-1}$  [4, 5], which exceeds the Planck value by more than  $4.4\sigma$ . This significant tension between early- and late-Universe measurements has only intensified in recent years.

Independent measurements using alternative methods have yielded intermediate or conflicting results. For instance, the Carnegie-Chicago Hubble Program (CCHP) reported a value of  $H_0 = 69.6 \pm 0.8 \pm 1.7 \text{ km s}^{-1}\text{Mpc}^{-1}$  based on the Tip of the Red Giant Branch (TRGB) method [8], which provides a distance calibration independent of Cepheids. Similarly, the H0LiCOW collaboration, using gravitational lensing time delays, reported two separate measurements:  $H_0 = 73.3^{+1.7}_{-1.8} \text{ km s}^{-1}\text{Mpc}^{-1}$  [9] and an updated value of  $H_0 = 75.3^{+3.0}_{-2.9} \text{ km s}^{-1}\text{Mpc}^{-1}$  [10].

Additional measurements from CMB lensing, variable stars, and other astrophysical probes further complicate the picture. Baxter et al. (2020) obtained a value of  $H_0 = 73.5 \pm 5.3 \text{ km s}^{-1}\text{Mpc}^{-1}$  from CMB lensing [12], while Huang et al. (2019) reported  $H_0 = 72.7 \pm 4.6 \text{ km s}^{-1}\text{Mpc}^{-1}$  using Miras (variable stars) [13]. These results underscore the ongoing difficulty in reconciling early- and late-Universe estimates of the Hubble constant, which remains one of the most significant challenges in modern cosmology. Addressing this discrepancy requires exploring new physics beyond the standard cosmological model, including modifications to gravity, dark energy models, and possible systematic errors in observational data. This discrepancy can be interpreted as a mismatch between early and late Universe observations [6]. Another significant tension arises from measurements of the  $\sigma_8$  parameter, which reflects the amplitude of matter density fluctuations on scales of  $8h^{-1}$  Mpc, where  $h$  is the reduced Hubble constant. A related parameter,

---

\* Email: yarahmadimohammad10@gmail.com

$S_8$ , is commonly used to quantify the strength of matter density fluctuations and is defined as:  $S_8 = \sigma_8 \sqrt{\frac{\Omega_m}{0.3}}$ , where  $\Omega_m$  is the matter density parameter. The parameter  $S_8$  provides a useful measure of the amplitude of density fluctuations in the universe and plays a crucial role in understanding cosmological structure formation. Matter density fluctuations seed the formation of cosmic structures, such as galaxies and galaxy clusters. By comparing measurements of large-scale structures from galaxy surveys and cosmic microwave background (CMB) data with theoretical predictions,  $S_8$  serves as a key parameter for constraining cosmological models.

The value inferred from the Planck CMB measurement is  $S_8 = 0.832 \pm 0.013$ . However, there exists a  $2\sigma$  tension with measurements from galaxy clusters and weak lensing. In our analysis, we also consider Gaussian priors on  $S_8$  based on measurements from KiDS-1000x{2dFLenS+BOSS} ( $S_8 = 0.766^{+0.02}_{-0.014}$ ) [22] and DES-Y3 ( $S_8 = 0.776 \pm 0.017$ ) [21].

The standard  $\Lambda$  Cold Dark Matter ( $\Lambda$ CDM) model, while providing a compelling explanation for many cosmological phenomena, faces several challenges, including the cosmic coincidence and fine-tuning problems. Alternative approaches to addressing these issues generally fall into two broad categories. The first class of models focuses on modifying the properties of the matter field, leading to dynamic dark energy models such as quintessence [50], tachyon [51], k-essence [52], phantom [53], Chaplygin gas [54], holographic dark energy [55–57], and agegraphic dark energy [58, 59], among others.

The second category of modifications arises from extending the geometric foundations of general relativity. These include  $f(R)$  gravity [60],  $f(T)$  gravity [61],  $f(R, T)$  theory [62], Brans-Dicke theory [63], Gauss-Bonnet gravity [64], Lovelock gravity [65], and Horava-Lifshitz gravity [66–69].

These alternative models and theories offer promising avenues to address the Hubble tension, suggesting that new physics beyond the standard  $\Lambda$ CDM paradigm may be required to fully understand the evolution of our Universe. An alternative explanation that has garnered significant attention in addressing the accelerated expansion of the universe is  $f(R)$  gravity. This theoretical framework predicts an expansion history that closely mirrors that of the standard  $\Lambda$ CDM model while simultaneously offering distinct predictions for the formation and evolution of cosmic structures. Within the domain of Riemannian geometry,  $f(R)$  gravity is regarded as a natural extension of General Relativity (GR), wherein the Einstein-Hilbert action is modified by replacing the Ricci scalar  $R$  with a more general function of  $R$ . This approach has been widely explored in numerous studies [70–77].

The motivation for investigating perturbed  $f(R)$  gravity and its interaction with neutrinos in the context of the Hubble tension arises from the increasing recognition that extensions of the standard  $\Lambda$ CDM model may hold the key to resolving this longstanding discrepancy. The Hubble tension, characterized by divergent measurements of  $H_0$  from early-universe probes such as the cosmic microwave background (CMB) and late-universe observations like Type Ia supernovae, indicates a potential need for new physics beyond GR. Perturbed  $f(R)$  gravity introduces modifications to the Einstein-Hilbert action, impacting both the background expansion and the evolution of cosmological perturbations. This added flexibility enables adjustments to cosmic evolution in a way that may reconcile the conflicting  $H_0$  measurements.

Furthermore, coupling  $f(R)$  gravity with neutrinos introduces additional dynamical effects, as neutrinos play a crucial role in the universe's energy budget, influencing both relativistic and non-relativistic phases of cosmic evolution. This interaction can alter key observables, including the sound horizon and matter clustering, which are essential in determining  $H_0$ . By incorporating the interplay between modified gravity and neutrino physics, these models provide a promising and testable framework to bridge the gap between early- and late-universe measurements. This approach presents a compelling avenue for addressing the Hubble tension and advancing our understanding of the fundamental laws governing cosmic expansion.

## II. $f(r)$ GRAVITY MODEL

$f(R)$  gravity is a compelling alternative to Einstein's General Theory of Relativity, offering a modified framework for understanding gravity and cosmic evolution. In this approach, the standard Einstein-Hilbert action is extended by replacing the Ricci scalar  $R$  with a general function  $f(R)$ , which allows for a richer variety of gravitational dynamics. The Ricci scalar itself encapsulates information about the curvature of spacetime, and by modifying its functional form,  $f(R)$  gravity provides new avenues to explain cosmic acceleration, structure formation, and potential deviations from General Relativity [14, 16, 17, 73].

One of the key motivations behind  $f(R)$  gravity is its ability to naturally account for the accelerated expansion of the universe without requiring a cosmological constant. Instead of postulating an exotic dark energy component, the modifications introduced in  $f(R)$  gravity effectively generate repulsive gravitational effects at large scales. Different choices of the function  $f(R)$  lead to various viable cosmological models, some of which successfully reproduce the

observed expansion history while also making unique predictions for large-scale structure growth.

Another significant aspect of  $f(R)$  gravity is its potential to resolve discrepancies in cosmological observations. The theory modifies the equations governing the evolution of density perturbations, which can have measurable effects on galaxy clustering and cosmic shear. Moreover, since  $f(R)$  gravity introduces additional scalar degrees of freedom, it provides a testable framework through precision gravitational experiments and astrophysical observations.

In addition to its cosmological implications,  $f(R)$  gravity has been extensively studied in the context of black hole physics, gravitational waves, and modified gravity phenomenology. Various formulations of the theory, including metric and Palatini approaches, yield different predictions for gravitational dynamics and observational signatures. The action for an  $f(R)$  gravity model in the attendance of matter components are given by

$$S = \frac{1}{16G\pi} \int d^4x \sqrt{(-g)}(R + f(R)) \quad (1)$$

Where  $R$  is the curved scalar. The equations for motion are:

$$\begin{aligned} G_{\mu\nu} - \frac{1}{2}g_{\mu\nu}f(R) + R_{\mu\nu}f_R(R) - g_{\mu\nu}(f_R(R)) + \\ f_R(R)_{\mu\nu} = -8\pi GT_{\mu\nu} \end{aligned} \quad (2)$$

Which is  $(f_R(R)) = \frac{df_R}{dR}$ . For the Robertson-Walker flat metric we have:

$$\frac{3\mathcal{H}'}{a^2}(1 + f_R) - \frac{1}{2}(R_0 + f_0) - \frac{3\mathcal{H}}{a^2}f_R' = -8\pi G\rho_0 \quad (3)$$

$$\begin{aligned} \frac{1}{a^2}(\mathcal{H}' + 2H^2)(1 + f_R) - \frac{1}{2}(R_0 + f_0) \\ - \frac{1}{a^2}(\mathcal{H}f_R' + f_R'') = 8\pi Gc_s^2\rho_0 \end{aligned} \quad (4)$$

Where  $R_0$  represents the scalar curvature corresponding to the non-perturbation metric,  $f_0 = f(R_0)$  and  $(f_R(R)) = \frac{df(R)}{dR}$  and prim means the derivative of the time ratio  $\eta$ .

$$2(1 + f_R)(-\mathcal{H}' + \mathcal{H}^2) + 2Hf_R' - f_R'' = 8\pi G\rho_0(1 + c_s^2)a^2 \quad (5)$$

finally, we come to the equation of conservation:

$$\rho_0' + 3(1 + c_s^2)\mathcal{H}\rho_0 = 0 \quad (6)$$

### Scalar perturbation

Consider a flat FRW metric scalar perturbation at the length and specific time scale:

$$ds^2 = a^2(\eta)((1 + 2\phi)d\eta^2 - (1 - 2\psi)dx^2) \quad (7)$$

$\phi \equiv \phi(\eta, x)$  and  $\psi \equiv \psi(\eta, x)$  are scalar disorders. The disturbed components of the energy-momentum tensor in this module are as follows:

$$\begin{aligned} \hat{\delta}T_0^0 = \hat{\delta}\rho = \rho_0\delta, \hat{\delta}T_j^i = -\hat{\delta}p\delta_j^i = -c_s^2\rho_0\delta_j^i\delta, \hat{\delta}p\delta_0^i = \\ - (1 + c_s^2)\rho_0\partial_i v \end{aligned} \quad (8)$$

Where  $V$  represents the potential value for velocity disturbances. The first-order disturbed equations, assuming the background equations are kept, are as follows:

$$\begin{aligned} (1 + f_R)\delta G_v^\mu + (R_{0v}^\mu + \nabla^\mu\nabla_v - \delta_v^\mu)f_{RR}\delta R + \\ ((\delta g^{\mu\alpha})\nabla_v\nabla_\alpha - \delta_v^\mu(\delta g^{\alpha\beta})\nabla_\alpha\nabla_\beta)f_R - \\ (g_0^{\alpha\mu}(\delta\Gamma_{\alpha v}^\gamma) - \delta_v^\mu g_0^{\alpha\beta})\partial_\gamma f_R = -8\pi G\delta T_v^\mu \end{aligned} \quad (9)$$

in above relations  $f_{RR} = \frac{d^2 f(R_0)}{dR_0^2}$  and  $= \nabla_\alpha \nabla^\alpha$  the invariant derivative of the metric ratio is not disturbed. The first-order disturbed equations in the universe during dust dominate,  $c_s^2 = 0$  are obtained as follows:

$$\phi - \psi = -\frac{f_{RR}}{1 + f_R} \hat{\delta}R \quad (10)$$

$$\begin{aligned} \hat{\delta}R = & -\frac{2}{a^2} (3\psi'' + 6(\mathcal{H}' + \mathcal{H}^2)\phi + \\ & 3\mathcal{H}(\phi' + 3\psi') - k^2(\phi - 2\psi)) \end{aligned} \quad (11)$$

$$\begin{aligned} (3\mathcal{H}(\phi' + \psi') + k^2(\phi + \psi) + 3\mathcal{H}'\psi - (3\mathcal{H}' - 6\mathcal{H}^2)\phi) \\ (1 + f_R) + (9\mathcal{H}\phi - 3\mathcal{H}\psi + 3\psi')f'_R = -a^2\delta\rho_0\kappa^2 \end{aligned} \quad (12)$$

$$\begin{aligned} (\phi'' + \psi'' + 3\mathcal{H}(\phi' + \psi') + 3\mathcal{H}'\phi + (\mathcal{H}' + 2\mathcal{H}^2)\phi) \\ (1 + f_R) + (3\mathcal{H}\phi - \mathcal{H}\psi + 3\phi')f'_R + (3\phi - \psi)f''_R = 0 \end{aligned} \quad (13)$$

$$\begin{aligned} (2\phi - \psi)f'_R + (\phi' + \psi' + \mathcal{H}(\phi + \psi))(1 + f_R) = \\ -a^2v\rho_0\kappa^2 \end{aligned} \quad (14)$$

$$\delta' - k^2v - 3\psi' = 0 \quad (15)$$

$$\phi + \mathcal{H}v + v' = 0 \quad (16)$$

### III. PERTURBED $f(R)$ GRAVITY COUPLED WITH NEUTRINOS

In this study, we investigate the interaction between neutrinos and modified gravity within the framework of  $f(R)$  gravity. The action governing the system is given by [101]

$$S = \int d^4x \sqrt{-g} \left[ \frac{1}{2\kappa^2} f(R) + \mathcal{L}_m + \mathcal{L}_{\text{int}} \right], \quad (17)$$

where  $f(R)$  is a general function of the Ricci scalar  $R$ ,  $\mathcal{L}_m$  and  $\mathcal{L}_\nu$  represent the Lagrangians of standard matter and neutrinos, respectively, and  $\mathcal{L}_{\text{int}}$  encodes the interaction between neutrinos and the modified gravitational field.

The variation of this action with respect to the metric tensor  $g_{\mu\nu}$  leads to the modified Einstein field equations:

$$f_R R_{\mu\nu} - \frac{1}{2} f(R)g_{\mu\nu} + (g_{\mu\nu}\square - \nabla_\mu \nabla_\nu)f_R = \kappa^2(T_{\mu\nu}^{(m)} + T_{\mu\nu}^{(\text{int})}), \quad (18)$$

where  $f_R = \frac{df}{dR}$ ,  $\square = \nabla^\alpha \nabla_\alpha$  is the d'Alembertian operator, and  $T_{\mu\nu}^{(m)}$ , and  $T_{\mu\nu}^{(\text{int})}$  denote the energy-momentum tensors for standard matter, neutrinos, and their interaction, respectively.

The effective energy-momentum tensor for neutrinos incorporates their coupling to the modified gravitational field, leading to a modified continuity equation:

$$\nabla^\mu T_{\mu\nu}^{(\nu)} = Q_\nu u_\nu, \quad (19)$$

where the coupling term is parameterized as

$$Q_\nu = -\Gamma \rho_\nu, \quad \text{with} \quad \Gamma = u^\mu \nabla_\mu f_R. \quad (20)$$

This parameter  $\Gamma$  governs the rate at which energy is exchanged between neutrinos and the modified gravitational field, reflecting how neutrinos respond to deviations from General Relativity. The explicit form of  $\Gamma$  depends on the specific  $f(R)$  model under consideration.

The conservation equation for neutrinos, incorporating this interaction, takes the form

$$\frac{d\rho_\nu}{dN} + 3(1+w_\nu)\rho_\nu = -\Gamma\rho_\nu, \quad (21)$$

where  $N = \ln a$  and  $w_\nu = P_\nu/\rho_\nu$  is the equation-of-state parameter for neutrinos. This equation describes the evolution of neutrino energy density in the presence of modified gravity effects.

The interaction between neutrinos and the modified gravitational field plays a crucial role in cosmic evolution, particularly in addressing the Hubble tension. By modifying the expansion history, this interaction provides an alternative mechanism for explaining late-time cosmic acceleration without invoking additional exotic dark energy components. Given their weakly interacting nature, neutrinos serve as sensitive probes of deviations from General Relativity, offering a potential avenue to test  $f(R)$  gravity and its implications for fundamental physics.

These theoretical developments, combined with observational constraints, enable us to explore the interplay between modified gravity and neutrino dynamics, shedding light on unresolved tensions in cosmology [101].

#### IV. HU-SAWICKI $f(R)$ GRAVITY MODEL

The Hu-Sawicki  $f(R)$  gravity model is a well-established modification of General Relativity designed to explain cosmic acceleration without invoking a cosmological constant. The model introduces a function  $f(R)$  that modifies the Einstein-Hilbert action, allowing deviations from General Relativity at low curvatures while recovering it at high curvatures. The functional form of  $f(R)$  in the Hu-Sawicki model is given by:

$$f(R) = -m^2 \frac{c_1 \left(\frac{R}{m^2}\right)^n}{c_2 \left(\frac{R}{m^2}\right)^n + 1} \quad (22)$$

where:

$m^2$  is a mass scale related to the cosmological constant,  $c_1$  and  $c_2$  are dimensionless parameters,  $n$  is a positive integer, often chosen to be  $n = 4$  for phenomenological reasons.

This form ensures that  $f(R)$  behaves like the cosmological constant  $\Lambda$  at low curvatures, but reduces to  $R$  (recovering General Relativity) at high curvatures. The model's key parameters,  $c_1$  and  $c_2$ , determine the behavior of the function at different curvature scales. The choice of  $n = 4$  allows for a smooth transition between different cosmic epochs, ensuring stability and avoiding ghost-like instabilities. This parametrization makes the model a strong candidate for explaining the late-time acceleration of the universe. The best-fit values for the Hu-Sawicki model parameters  $c_1$ ,  $c_2$ , and  $f_0$  were obtained using various cosmological dataset combinations. For the CMB+Lensing dataset, the parameters are  $c_1 = 1.24 \pm 0.08 \times 10^{-3}$ ,  $c_2 = 6.77 \pm 0.14 \times 10^{-5}$ , and  $f_0 = 0.994 \pm 0.007$ . When including Cosmic Chronometers (CC) in CMB+Lensing+CC, the best-fit values shift slightly to  $c_1 = 1.29 \pm 0.13 \times 10^{-3}$ ,  $c_2 = 6.72 \pm 0.14 \times 10^{-5}$ , and  $f_0 = 0.996 \pm 0.009$ . For the combination CMB+Lensing+BAO, the values are  $c_1 = 1.15 \pm 0.13 \times 10^{-3}$ ,  $c_2 = 6.42 \pm 0.17 \times 10^{-5}$ , and  $f_0 = 0.999 \pm 0.008$ . The CMB+Lensing+Pantheon dataset gives  $c_1 = 1.25 \pm 0.10 \times 10^{-3}$ ,  $c_2 = 6.63 \pm 0.16 \times 10^{-5}$ , and  $f_0 = 0.998 \pm 0.006$ . Finally, using the most comprehensive dataset, CMB+Lensing+All, the best-fit values are  $c_1 = 1.15 \pm 0.08 \times 10^{-3}$ ,  $c_2 = 6.55 \pm 0.08 \times 10^{-5}$ , and  $f_0 = 0.995 \pm 0.006$ .

These results consistently show that  $c_1$  remains on the order of  $10^{-3}$  and  $c_2$  around  $10^{-5}$ , with  $f_0$  close to unity across all dataset combinations. The overall agreement with previous studies further supports the validity of the Hu-Sawicki model in describing cosmic acceleration [101, 110]. The parameter  $\Gamma$  is explicitly written in terms of the Hu-Sawicki model [101]):

$$\Gamma = \frac{d}{dN} (f_R) = \frac{d}{dN} \left( \frac{-nc_1 \left(\frac{R}{m^2}\right)^{n-1}}{\left(c_2 \left(\frac{R}{m^2}\right)^n + 1\right)^2} \right) \quad (23)$$

Equations (12–14) constitute a set of nonlinear second-order differential equations involving multiple variables and parameters. Analytical solutions for such equations are generally unattainable, except in the simplest cases. To address this complexity, we transform these second-order equations into an equivalent system of first-order differential equations by introducing suitable new variables. This reformulation offers several advantages: first-order systems are more amenable to numerical computation and facilitate a more comprehensive analysis of the system's dynamics through phase space representations.

Phase space analysis plays a crucial role, particularly in oscillatory systems, where trajectories can exhibit behaviors such as spiraling towards the origin, diverging to infinity, or stabilizing at equilibrium points. This method is instrumental in evaluating the stability and qualitative behavior of the system. By redefining variables and parameters, we systematically restructure the field equations within the phase space framework, thereby simplifying their interpretation and analysis. This approach provides deeper insights into the underlying physical mechanisms and their stability properties, enhancing our understanding of the system's long-term evolution.

The new variables introduced for this transformation are generally defined as follows:

$$\begin{aligned}\eta_1 &= \frac{\phi'}{\phi H}, \eta_2 = \frac{\kappa}{H}, \eta_3 = \frac{f'_R}{H(1+f_R)}, \eta_4 = \frac{\delta}{\phi}, \\ \eta_5 &= \frac{\rho_m a^2}{(1+f_R)}, \eta_6 = \frac{\Psi'}{\phi H}, \eta_7 = \frac{\Psi}{\phi}, \eta_8 = \frac{\rho_\nu a^2}{(1+f_R)},\end{aligned}\quad (24)$$

Using the Hu-Sawicki form of  $f(R)$ , the previously defined autonomous equations are modified as follows. These equations describe the evolution of key dynamical variables in the system:

- **Evolution of  $\eta_1$  (Scalar Field Normalized Derivative):**

$$\frac{d\eta_1}{dN} = \chi_3 - \eta_1^2 - \eta_1 \quad (25)$$

where  $\eta_1$  represents the normalized derivative of the scalar field.

- **Evolution of  $\eta_2$  (Curvature-Hubble Ratio):**

$$\frac{d\eta_2}{dN} = -\eta_2 \chi_1 \quad (26)$$

where  $\eta_2$  quantifies the ratio of the Ricci curvature to the Hubble parameter.

- **Evolution of  $\eta_3$  (Modified Gravity Parameter):**

$$\frac{d\eta_3}{dN} = \beta - \eta_3^2 - \chi_1 \eta_3 \quad (27)$$

where  $\eta_3$  is defined as:

$$\eta_3 = \frac{f'_R}{H(1+f_R)} \quad (28)$$

and the function  $\beta$  is given by:

$$\beta = \frac{f''_R}{(1+f_R)H} - 1 \quad (29)$$

with  $f_R$  and  $f''_R$  derived from the Hu-Sawicki form of  $f(R)$ .

- **Evolution of  $\eta_4$  (Scalar Field Perturbation):**

$$\frac{d\eta_4}{dN} = \eta_4(1 - \eta_1) \quad (30)$$

where  $\eta_4$  governs perturbations in the scalar field.

- **Evolution of  $\eta_5$  (Matter Density Contribution):**

$$\frac{d\eta_5}{dN} = -\eta_5(1 + \eta_3) \quad (31)$$

where  $\eta_5$  describes the evolution of the matter density.

- **Evolution of  $\eta_6$  (Gravitational Potential Evolution):**

$$\frac{d\eta_6}{dN} = \chi_2 - \eta_6(\eta_1 + \chi_1) \quad (32)$$

where  $\eta_6$  characterizes the evolution of the gravitational potential.

- **Evolution of  $\eta_7$  (Additional Gravitational Potential Parameter):**

$$\frac{d\eta_7}{dN} = \eta_6 - \eta_7\eta_1 \quad (33)$$

where  $\eta_7$  is another parameter related to the gravitational potential.

- **Evolution of  $\eta_8$  (Neutrino Contribution):**

$$\frac{d\eta_8}{dN} = \eta_8(3\omega_\nu - 1) - \eta_3\eta_8 + \Gamma\eta_2\eta_8 \quad (34)$$

where  $\eta_8$  incorporates neutrino effects, and  $\Gamma$  represents a coupling term between neutrinos and the gravitational sector.

Where  $N = \ln a$  thus,  $\frac{d}{dN} = \frac{1}{H} \frac{d}{d\tau}$ .

The function  $\beta$  plays a fundamental role in the study of modified gravity theories, particularly in the framework of  $f(R)$  gravity. This parameter encapsulates deviations from General Relativity (GR) introduced by the modification function  $f(R)$ , which introduces additional dynamical degrees of freedom in the gravitational action. The term  $f''_R$ , representing the second derivative of  $f(R)$  with respect to the Ricci scalar  $R$ , is particularly significant as it governs the behavior of the scalar degree of freedom inherent in  $f(R)$  gravity.

The parameter  $\beta$  effectively quantifies departures from GR by measuring the relative contribution of the modified gravity terms in comparison to the standard Hubble expansion rate  $H$ . A value of  $\beta = -1$  corresponds to the case where no modifications exist, recovering standard GR. The evolution of  $\beta$  has profound implications for cosmic expansion and the growth of large-scale structures, influencing key cosmological observables such as the growth rate of matter perturbations and the dynamics of dark energy.

Comprehensive discussions on the theoretical foundations and cosmological implications of modified gravity, including  $f(R)$  models, can be found in [92, 94, 95].

After some calculation from equations, for simplicity, we can obtain the above parameters in terms of the new variables as

$$\chi_1 = \frac{\mathcal{H}'}{\mathcal{H}^2}, \chi_2 = \frac{\Psi''}{\phi H^2}, \chi_3 = \frac{\phi''}{\phi H^2}, \chi_4 = \frac{\delta'}{\phi H} \quad (35)$$

Now, for the autonomous equations of motions, we obtain

$$\begin{aligned} \chi_1 &= \frac{1}{1 - \eta_7} [\eta_1 + \eta_6 + \frac{1}{3}\eta_2^2(1 + \eta_7) + (3 - \eta_7 + \eta_6)\eta_5 + \\ &\quad (3 - \eta_7 + \eta_6)\eta_8 - \frac{\kappa^2}{k^2}\eta_5\eta_4\eta_2^2] \end{aligned} \quad (36)$$

$$\begin{aligned} \chi_2 &= \frac{-2}{1 - \eta_7} [\eta_1 + \eta_6 + \frac{1}{3}\eta_2^2(1 + \eta_7) + \\ &\quad (3 - \eta_7 + \eta_6)\eta_5 - \frac{\kappa^2}{k^2}\eta_5\eta_4\eta_2^2] \\ &\quad - \eta_1 - 3\eta_6 + \frac{1}{3}\eta_2^2 - \eta_6\eta_1 + \\ &\quad \frac{1}{3}\eta_2^2(1 - 2\eta_7) + \frac{\Omega}{3}(1 - \eta_7)\frac{1}{k^2}\eta_2^2 \end{aligned} \quad (37)$$

$$\begin{aligned}\chi_3 = & -\chi_2 - 3\chi_1\left(1 + \frac{1}{3}\eta_7\right) - 3\eta_1 - 3\eta_6 - 2\eta_7 - \\ & (3 - \eta_7 + 3\eta_1)\eta_5 + \beta(\eta_7 - 3)\end{aligned}\tag{38}$$

$$\chi_4 = \frac{-\kappa^2[(2 - \eta_7)\eta_3 + \eta_1 + \eta_6 + 1 + \eta_7]}{\kappa^2\eta_5} + 3\eta_6\tag{39}$$

The parameter  $\chi_1$  plays a crucial role in cosmological analysis, as it facilitates the expression of fundamental cosmological parameters, such as the deceleration parameter  $q$  and the effective equation of state parameter  $w_{\text{eff}}$ , in terms of its contributions. These parameters provide essential insights into the dynamical evolution of the Universe, particularly in understanding cosmic acceleration and the nature of dark energy.

The deceleration parameter  $q$  is a dimensionless quantity that quantifies the rate at which the expansion of the Universe is slowing down or accelerating. It is defined in terms of the Hubble parameter  $\mathcal{H}$  as:

$$q = -1 - \frac{\mathcal{H}'}{\mathcal{H}^2}\tag{40}$$

where  $\mathcal{H}$  is the Hubble parameter in conformal time, and  $\mathcal{H}'$  represents its derivative with respect to conformal time. A negative value of  $q$  corresponds to an accelerating Universe, as observed in the late-time cosmic expansion, while a positive  $q$  indicates deceleration.

Similarly, the effective equation of state parameter,  $w_{\text{eff}}$ , which characterizes the overall cosmic fluid, is expressed as:

$$w_{\text{eff}} = -1 - \frac{2}{3}\frac{\mathcal{H}'}{\mathcal{H}^2}\tag{41}$$

This equation provides insight into whether the Universe is dominated by dark energy, matter, or radiation at a given epoch.

Alternatively, in terms of the scale factor  $a(t)$ , the deceleration parameter is traditionally defined as:

$$q = -\frac{a''a}{(a')^2}\tag{42}$$

where  $a'$  and  $a''$  denote the first and second derivatives of the scale factor with respect to cosmic time. This form directly relates to the physical acceleration of the cosmic expansion, as a positive  $a''$  (implying  $q < 0$ ) signifies an accelerating Universe, which aligns with the observed late-time acceleration due to dark energy. Conversely, a decelerating Universe corresponds to  $q > 0$ , which was the case during the matter-dominated and radiation-dominated eras.

By parameterizing  $q$  and  $w_{\text{eff}}$  in terms of  $\chi_1$ , one gains a more structured approach to analyzing cosmic evolution, particularly in the context of modified gravity theories and alternative dark energy models.

## V. NUMERICAL ANALYSIS

In our analysis, we incorporate various observational datasets, including Type Ia Supernovae (SNe Ia), cosmic microwave background (CMB) anisotropies, CMB lensing, baryon acoustic oscillations (BAO), and cosmic chronometers (CC). A brief description of each dataset is provided below:

Pantheon+ Supernovae Data:

We utilize the Pantheon+ compilation, which consists of 896 SNe Ia spanning the redshift range  $0.12 < z < 2.3$  [78]. This dataset provides precise luminosity distance measurements and serves as a crucial probe for constraining the late-time expansion history of the universe [102].

CMB Anisotropy Data:

We include the most recent cosmic microwave background (CMB) temperature and polarization power spectra

Table I: 12 BAO measurements covering the redshift range  $0.122 \leq z \leq 2.334$ .

$z$	Measurement	Value
0.122	$D_V(r_{s,\text{fid}}/r_s)$	$539 \pm 17$
0.38	$D_M/r_s$	10.23406
0.38	$D_H/r_s$	24.98058
0.51	$D_M/r_s$	13.36595
0.51	$D_H/r_s$	22.31656
0.698	$D_M/r_s$	17.86
0.698	$D_H/r_s$	19.33
0.835	$D_M/r_s$	$18.92 \pm 0.51$
1.48	$D_M/r_s$	30.6876
1.48	$D_H/r_s$	13.2609
2.334	$D_M/r_s$	37.5
2.334	$D_H/r_s$	8.99

from the final release of Planck 2018. Specifically, we adopt the plikTTTEEE+lowl+lowE likelihood [80], which provides constraints on both early- and late-time cosmological parameters by analyzing temperature (TT), E-mode polarization (EE), and temperature-polarization cross-correlation (TE) power spectra.

#### CMB Lensing Data:

We also account for the Planck 2018 CMB lensing reconstruction power spectrum [82], obtained from a trispectrum analysis. This dataset probes the large-scale distribution of matter by measuring the gravitational lensing of CMB photons, thereby offering valuable constraints on the sum of neutrino masses and dark energy properties.

#### Baryon Acoustic Oscillations (BAO) Data:

To complement the CMB constraints, we include BAO measurements from various galaxy surveys ([103–109]). These BAO measurements serve as a standard ruler to probe the expansion history of the universe. The dataset consists of 12 BAO measurements covering the redshift range  $0.122 \leq z \leq 2.334$ , as listed in Table I. The key BAO quantities used in our analysis include:

-  $D_V(z)$ : The volume-averaged angular diameter distance, defined as

$$D_V(z) = [czH^{-1}(z)D_M^2(z)]^{1/3}. \quad (43)$$

-  $D_H(z)$ : The Hubble distance, given by  $D_H(z) = c/H(z)$ . -  $D_M(z)$ : The transverse comoving distance, which for a spatially flat universe is given by

$$D_M(z) = D_C(z) = c \int_0^z \frac{dz'}{H(z')}. \quad (44)$$

-  $r_s$ : The sound horizon at the drag epoch, with a fiducial value of  $r_{s,\text{fid}} = 147.5$  Mpc.

The detailed BAO measurements used in our analysis are presented in Table I.

#### Cosmic Chronometer (CC) Data:

We include 32 cosmic chronometer (CC) measurements of the Hubble parameter  $H(z)$  spanning the redshift range  $0.07 < z < 1.965$ , as listed in Table II. The CC technique provides model-independent constraints on  $H(z)$  by using the differential age method to determine the expansion rate of the universe at different epochs.

By combining these complementary datasets, we obtain robust constraints on cosmological parameters, allowing us to test the viability of our theoretical models.

## VI. DATA INTEGRATION AND LIKELIHOOD FUNCTIONS IN MONTEPYTHON

MontePython [111, 112] is a flexible cosmological inference framework that interfaces with the Boltzmann code CLASS [113] and supports a wide range of cosmological and astrophysical likelihoods. It enables robust parameter estimation through Bayesian inference using Markov Chain Monte Carlo (MCMC) or nested sampling techniques.

The total likelihood for a given parameter set  $\theta$  is constructed as the product of individual likelihoods:

$$\mathcal{L}(\text{data}|\theta) = \mathcal{L}_{\text{CMB}} \times \mathcal{L}_{\text{CC}} \times \mathcal{L}_{\text{BAO}} \times \mathcal{L}_{\text{SN}} \times \mathcal{L}_{\text{lensing}}, \quad (45)$$

with each term representing the likelihood contribution from an independent cosmological probe.

Table II: 32  $H(z)$  (CC) data.

$z$	$H(z)$	$\sigma$
0.07	69.0	19.6
0.09	69.0	12.0
0.12	68.6	26.2
0.17	83.0	8.0
0.2	72.9	29.6
0.27	77.0	14.0
0.28	88.8	36.6
0.4	95.0	17.0
0.47	89.0	50.0
0.48	97.0	62.0
0.75	98.8	33.6
0.88	90.0	40.0
0.9	117.0	23.0
1.3	168.0	17.0
1.43	177.0	18.0
1.53	140.0	14.0
1.75	202.0	40.0
0.1791	74.91	4.00
0.1993	74.96	5.00
0.3519	82.78	14
0.3802	83.0	13.5
0.4004	76.97	10.2
0.4247	87.08	11.2
0.4497	92.78	12.9
0.4783	80.91	9
0.5929	103.8	13
0.6797	91.6	8
0.7812	104.5	12
0.8754	125.1	17
1.037	153.7	20
1.363	160.0	33.6
1.965	186.5	50.4

### CMB Likelihoods

`MontePython` incorporates official likelihoods from Planck 2018 [114]. The likelihood is constructed from differences between observed and theoretical CMB temperature and polarization power spectra:

$$\mathcal{L}_{\text{CMB}} \propto \exp\left(-\frac{1}{2}\Delta\mathbf{C}_\ell^T \mathbf{C}_{\text{CMB}}^{-1} \Delta\mathbf{C}_\ell\right), \quad (46)$$

where  $\Delta\mathbf{C}_\ell = \mathbf{C}_\ell^{\text{obs}} - \mathbf{C}_\ell^{\text{theory}}$ , and  $\mathbf{C}_{\text{CMB}}$  is the covariance matrix for the angular power spectra.

### Cosmic Chronometers (CC)

The CC likelihood utilizes Hubble parameter measurements  $H(z)$  derived from differential aging of passively evolving galaxies. The likelihood function takes the Gaussian form:

$$\mathcal{L}_{\text{CC}} \propto \exp\left(-\frac{1}{2}\Delta\mathbf{H}^T \mathbf{C}_{\text{CC}}^{-1} \Delta\mathbf{H}\right), \quad (47)$$

where  $\Delta\mathbf{H} = \mathbf{H}_{\text{obs}} - \mathbf{H}_{\text{model}}$ , and  $\mathbf{C}_{\text{CC}}$  is the diagonal or full covariance matrix depending on the dataset used. Integration of CC data into `MontePython` is straightforward via the `data/ likelihood` module.

### Baryon Acoustic Oscillations (BAO)

BAO data constrain cosmological distances via features imprinted in the galaxy correlation function. `MontePython` includes likelihoods from 6dFGS, SDSS MGS, BOSS DR12, and eBOSS. The likelihood compares observed and theoretical distance combinations:

$$\mathcal{L}_{\text{BAO}} \propto \exp\left(-\frac{1}{2}\Delta\mathbf{D}^T \mathbf{C}_{\text{BAO}}^{-1} \Delta\mathbf{D}\right), \quad (48)$$

where  $\Delta\mathbf{D} = \mathbf{D}_{\text{obs}} - \mathbf{D}_{\text{model}}$  includes quantities like  $D_V(z)$ ,  $D_M(z)$ , and  $H(z)$ , with  $\mathbf{C}_{\text{BAO}}$  as the associated covariance.

Table III: Flat priors for the cosmological parameters.

Parameter	Prior
$\Omega_b h^2$	[0.00, 0.10]
$\Omega_c h^2$	[0.00, 0.15]
$\tau$	[0.00, 0.80]
$n_s$	[0.80, 1.20]
$\log[10^{10} A_s]$	[1.60, 3.90]
$100\theta_{MC}$	[0.50, 10.50]
$\Omega_\nu$	[0.00, 0.009]

### Type Ia Supernovae (Pantheon)

The Pantheon sample [115] is implemented in `MontePython` through binned or unbinned distance modulus likelihoods:

$$\mathcal{L}_{\text{SN}} \propto \exp \left( -\frac{1}{2} \sum_j \frac{(\mu_j^{\text{obs}} - \mu_j^{\text{model}})^2}{\sigma_\mu(j)^2} \right), \quad (49)$$

where  $\mu_j^{\text{obs}}$  and  $\mu_j^{\text{model}}$  are the observed and predicted distance moduli, respectively, and  $\sigma_\mu(j)$  denotes the measurement uncertainties. Full covariance support is also available for high-precision analyses.

### CMB Lensing

Lensing likelihoods constrain projected matter distributions and are available via Planck [114] and other CMB experiments. The likelihood is computed from:

$$\mathcal{L}_{\text{lensing}} \propto \exp \left( -\frac{1}{2} \Delta \mathbf{d}_{\text{lens}}^T \mathbf{C}_{\text{lens}}^{-1} \Delta \mathbf{d}_{\text{lens}} \right), \quad (50)$$

where  $\Delta \mathbf{d}_{\text{lens}} = \mathbf{d}_{\text{obs}} - \mathbf{d}_{\text{theory}}$  corresponds to lensing deflection spectra or convergence maps, and  $\mathbf{C}_{\text{lens}}$  is the covariance matrix.

### Posterior Sampling and Chi-Squared Evaluation

`MontePython` performs MCMC sampling using the Metropolis–Hastings algorithm, optionally with adaptive proposals and fast sampling modes. The posterior is defined as:

$$\mathcal{P}(\theta | \text{data}) \propto \mathcal{L}(\text{data} | \theta) \cdot \pi(\theta), \quad (51)$$

where  $\pi(\theta)$  denotes the priors. A typical choice includes flat or logarithmic priors depending on physical parameter ranges.

The corresponding total chi-squared is given by:

$$\chi_{\text{total}}^2 = \sum_i \chi_i^2 = \sum_i -2 \ln \mathcal{L}_i, \quad (52)$$

where  $\chi_i^2$  corresponds to each likelihood contribution. The best-fit parameters minimize  $\chi_{\text{total}}^2$ , while confidence intervals are derived from the marginalized posterior.

Table IV shows the flat priors for the cosmological parameters based on ([79] ; [81]; [82]; [91]; [90])

## VII. CONSTRAINT ON THE TOTAL MASS OF NEUTRINOS

The behavior of neutrinos—elusive and enigmatic particles—is significantly influenced by modifications to gravitational dynamics, such as those introduced in perturbed  $f(R)$  gravity [95]. In this section, we analyze the constraints on the total mass of neutrinos within this framework. A key equation governing the energy density of neutrinos ( $\rho_\nu$ ), the scale factor ( $a$ ), and the modification term ( $1 + f_R$ ) is given by [92, 94]:

$$\eta_9 = \frac{\rho_\nu a^2}{(1 + f_R)}. \quad (53)$$

To extract meaningful constraints on the total neutrino mass, additional physical assumptions and observational inputs are required. The energy density of neutrinos can be expressed in terms of their mass ( $m_\nu$ ) and temperature ( $T_\nu$ ). A common approach utilizes the Fermi-Dirac distribution for relativistic neutrinos, yielding [93, 96]:

$$\rho_\nu = \frac{7\pi^2}{120} g_\nu T_\nu^4, \quad (54)$$

where  $g_\nu$  denotes the number of degrees of freedom for neutrinos, typically taken as 2 per neutrino species. Substituting this expression into Equation (1), we obtain:

$$\eta_9 = \frac{\left(\frac{7\pi^2}{120} g_\nu T_\nu^4\right) a^2}{(1 + f_R)}. \quad (55)$$

The sum of neutrino masses, a fundamental parameter in cosmology, is linked to the neutrino density parameter  $\Omega_\nu$  via the following relationship [96]:

$$\Omega_\nu = \frac{\sum m_\nu}{94h^2}. \quad (56)$$

To determine the total mass of neutrinos,  $\sum m_\nu$ , we must accurately estimate the cosmological parameters  $\Omega_\nu$  and  $h$ . This is typically achieved through Bayesian inference techniques, specifically using the Markov Chain Monte Carlo (MCMC) method.

The MCMC approach involves defining a cosmological model with a set of free parameters, including the neutrino mass, and constructing a likelihood function based on observational datasets such as Cosmic Microwave Background (CMB) anisotropies, Baryon Acoustic Oscillations (BAO), Cosmic Chronometers (CC), and Pantheon supernova data. The likelihood function is expressed as:

$$\mathcal{L} \propto \exp\left(-\frac{1}{2} \sum_i \left[ \frac{D_i^{\text{obs}} - D_i^{\text{model}}}{\sigma_{D_i}} \right]^2\right), \quad (57)$$

where  $D_i$  represents different cosmological observables and  $\sigma_{D_i}$  their corresponding uncertainties. The MCMC sampling explores the parameter space, assigning prior distributions to parameters such as  $\sum m_\nu$ ,  $\Omega_\nu$ , and  $h$ . The best-fitting values are obtained by maximizing the posterior probability:

$$P(\theta|\text{data}) \propto \mathcal{L}(\text{data}|\theta) \cdot P(\theta), \quad (58)$$

where  $P(\theta)$  represents the prior probability distribution of the parameters. The MCMC analysis produces marginalized posterior distributions, providing credible intervals for the total neutrino mass.

In Fig. 1 (top panel), the constraints on the total neutrino mass,  $\sum m_\nu$ , and the Hubble constant,  $H_0$ , are presented for various dataset combinations within the framework of the perturbed  $f(R) + m_\nu$  model. Given the lower bound of  $\sum m_\nu = 0.06$  eV from neutrino oscillation experiments, it is evident that the constraints on  $H_0$  exhibit a strong dependence on  $\sum m_\nu$ , particularly when the Cosmic Microwave Background (CMB) data is included.

Table IV: Cosmological Parameter Results for Different Datasets for perturbed  $f(R)$  gravity

Parameter	CMB+Pantheon+Lensing	CMB+CC+Lensing	CMB+BAO+Lensing	CMB+Lensing	CMB+ALL
$\Omega_b h^2$	$0.02226 \pm 0.00022$	$0.02228 \pm 0.00023$	$0.02234 \pm 0.00020$	$0.02236 \pm 0.00021$	$0.02219 \pm 0.00018$
$\Omega_c h^2$	$0.1196 \pm 0.0037$	$0.1194 \pm 0.0041$	$0.1191 \pm 0.0035$	$0.1194 \pm 0.0035$	$0.1187 \pm 0.0025$
$100\theta_{MC}$	$1.0410 \pm 0.0006$	$1.0408 \pm 0.0007$	$1.0411 \pm 0.0006$	$1.04115 \pm 0.0005$	$1.0408 \pm 0.0005$
$\tau$	$0.059 \pm 0.008$	$0.061 \pm 0.009$	$0.0551 \pm 0.008$	$0.055 \pm 0.008$	$0.054^{+0.006}_{-0.007}$
$\ln(10^{10} A_s)$	$3.047 \pm 0.02$	$3.045 \pm 0.017$	$3.043 \pm 0.019$	$3.046 \pm 0.018$	$3.042^{+0.016}_{-0.017}$
$n_s$	$0.971 \pm 0.009$	$0.970 \pm 0.009$	$0.974 \pm 0.008$	$0.964 \pm 0.008$	$0.969 \pm 0.007$

Analyzing different dataset combinations, we find that the most stringent upper bound on the total neutrino mass at the 95% confidence level (CL) is obtained when considering the full combination of datasets, yielding  $\sum m_\nu < 0.119$  eV. This results are in broad agreement with [3]. The inclusion of additional observational probes such as cosmic chronometers (CC), baryon acoustic oscillations (BAO), and the Pantheon supernova sample progressively refines the constraints, highlighting the role of complementary data in constraining both  $\sum m_\nu$  and  $H_0$ .

Furthermore, Fig. 1, (low panel) illustrates the constraints on the interaction parameter  $\Gamma$  and the Hubble constant  $H_0$  across different dataset combinations. Our analysis shows that the most precise determination of  $\Gamma$  is achieved when utilizing the full dataset combination, yielding  $\Gamma = 0.64 \pm 0.14$ .

For a comprehensive understanding, the numerical constraints on  $\Gamma$  and  $\sum m_\nu$  for various dataset combinations are as follows:

CMB + Lensing:  $\Gamma = 0.62 \pm 0.32$ ,  $\sum m_\nu < 0.32$  eV CMB + BAO + Lensing:  $\Gamma = 0.64 \pm 0.15$ ,  $\sum m_\nu < 0.131$  eV CMB + CC + Lensing:  $\Gamma = 0.641 \pm 0.14$ ,  $\sum m_\nu < 0.142$  eV CMB + Pantheon + Lensing:  $\Gamma = 0.62 \pm 0.31$ ,  $\sum m_\nu < 0.29$  eV CMB + CC + BAO + Pantheon + Lensing:  $\Gamma = 0.64 \pm 0.14$ ,  $\sum m_\nu < 0.119$  eV in 68 % confidence level.

These results emphasize the crucial role of combining multiple observational datasets in refining cosmological constraints, particularly in assessing the contribution of neutrinos to the cosmic energy budget. The consistency of the obtained bounds with current cosmological constraints further reinforces the validity of the perturbed  $f(R) + m_\nu$  model in describing late-time cosmic evolution.

### VIII. HUBBLE TENSION ANALYSIS

The discrepancies in Hubble constant ( $H_0$ ) measurements are evaluated using the tension equation, which quantifies the disagreement between different datasets relative to the Planck 2018 and R22 results in terms of standard deviations ( $\sigma$ ). Table IX provides a comparative analysis of  $H_0$  across various datasets, presenting their values, uncertainties, and tensions concerning Planck 2018 and R22, with uncertainties representing standard deviations in km/s/Mpc for the perturbed  $f(R)$  gravity model. Additionally, Table VII summarizes the cosmological parameter constraints derived from different dataset combinations, including the Cosmic Microwave Background (CMB) alongside Pantheon, cosmic chronometers (CC), Baryon Acoustic Oscillations (BAO), lensing, and an all-encompassing combination (CMB+ALL), demonstrating how these datasets synergistically refine parameter estimates and enhance precision. The influence of these combinations is crucial in mitigating uncertainties and strengthening constraints within the perturbed  $f(R)$  gravity framework, underscoring how diverse datasets complement one another in improving cosmological inferences. The key cosmological parameters presented in Table VII define the universe's evolution and structure, including  $\Omega_b h^2$  and  $\Omega_c h^2$ , which describe the physical densities of baryonic and cold dark matter, respectively;  $100\theta_{MC}$ , which represents the angular size of the sound horizon at last scattering;  $\tau$ , the optical depth to reionization;  $\ln(10^{10} A_s)$ , the logarithm of the primordial scalar perturbation amplitude; and  $n_s$ , the scalar spectral index characterizing the scale dependence of primordial fluctuations. These parameters are fundamental in constraining theoretical models like  $f(R)$  gravity, offering deeper insights into the universe's fundamental properties and the impact of dataset combinations on cosmological analyses.

#### Hubble Tension Analysis in Perturbed $f(R)$ Gravity

In this study, we investigate the Hubble constant ( $H_0$ ) within the framework of the perturbed  $f(R)$  gravity model, employing various observational dataset combinations. Table V presents a comparative analysis of the derived  $H_0$

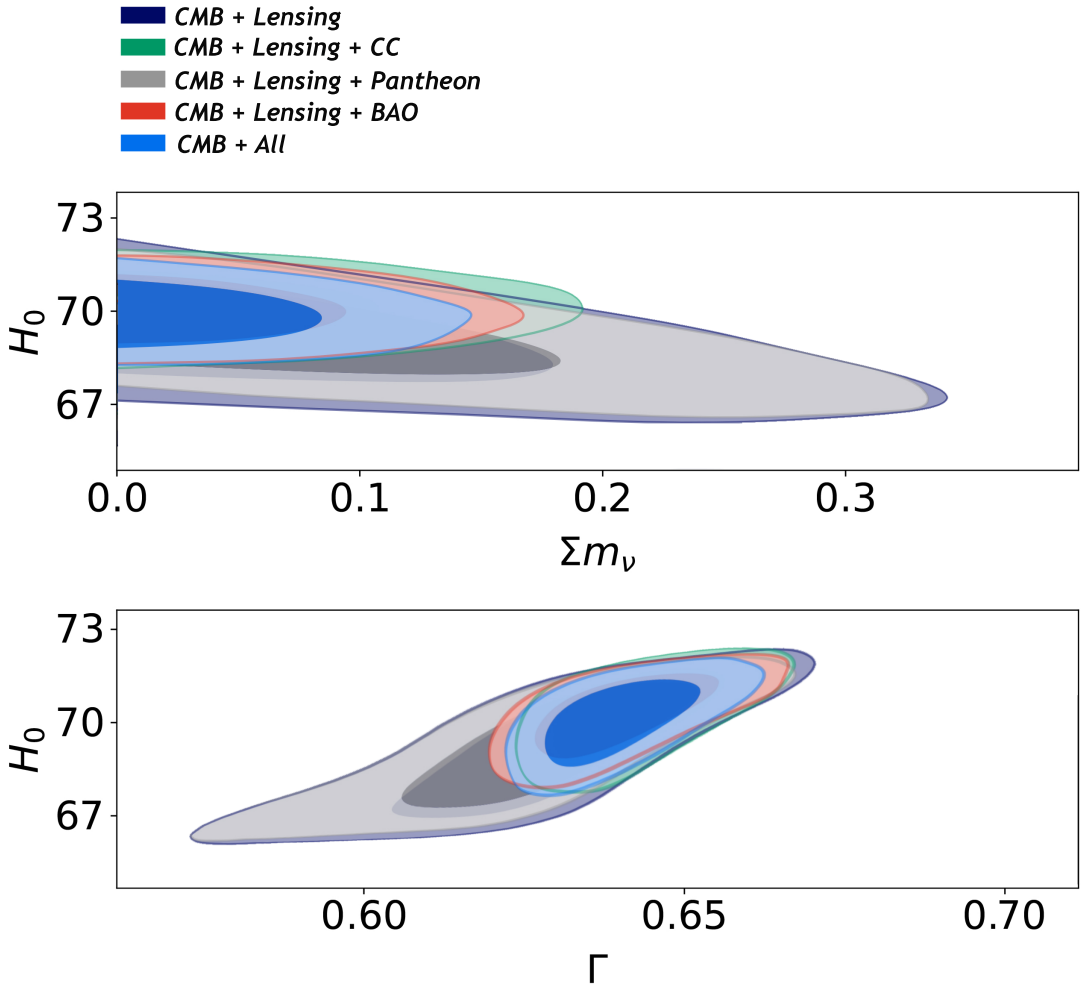


Figure 1: Top panel: The comparison of  $\sum m_\nu$ , and  $H_0$ . Low panel: The comparison of  $\Gamma$ , and  $H_0$  from the variety of dataset combination in perturbed  $f(R) + m_\nu$  model

values against the established Planck 2018 measurement ( $H_0^{\text{Planck 2018}} = 67.4 \pm 0.5 \text{ km/s/Mpc}$ ) [3] and the R22 result ( $H_0^{\text{R22}} = 73.5 \pm 1.04 \text{ km/s/Mpc}$ ), highlighting the corresponding statistical tensions.

For the Cosmic Microwave Background (CMB) and lensing combination, we obtain  $H_0 = 69.6 \pm 2.8 \text{ km/s/Mpc}$ , resulting in a mild tension of  $0.61\sigma$  with Planck 2018 and  $1.26\sigma$  with R22. This suggests that while the CMB+lensing dataset moderately reconciles both early and late Universe determinations, it does not completely resolve the discrepancy.

When Baryon Acoustic Oscillations (BAO) data are included alongside CMB and lensing, the inferred Hubble constant rises to  $H_0 = 70.15 \pm 1.6 \text{ km/s/Mpc}$ . This combination increases the tension with Planck to  $1.23\sigma$ , while slightly reducing the tension with R22 to  $1.18\sigma$ , indicating that the inclusion of BAO does not significantly alleviate the Hubble tension but brings slight consistency with local distance ladder measurements.

Incorporating cosmic chronometers (CC) data along with CMB and lensing results in  $H_0 = 70.52 \pm 1.92 \text{ km/s/Mpc}$ , leading to a  $1.15\sigma$  deviation from Planck and  $1.22\sigma$  from R22. The CC dataset marginally shifts the results towards the local value but still maintains a comparable level of disagreement with both measurements.

Additionally, adding Pantheon (Type Ia Supernovae) data to the CMB and lensing datasets yields  $H_0 = 70.88 \pm 1.94 \text{ km/s/Mpc}$ , increasing the tension with Planck to  $1.22\sigma$  while reducing the discrepancy with R22 to  $1.10\sigma$ . This

Dataset Combination	$H_0$ Value (km/s/Mpc)	Tension with Planck 2018	Tension with R22
CMB + Lensing	$69.6 \pm 2.8$	$0.61\sigma$	$1.26\sigma$
CMB + BAO + Lensing	$70.15 \pm 1.6$	$1.23\sigma$	$1.18\sigma$
CMB + Lensing + CC	$70.52 \pm 1.92$	$1.15\sigma$	$1.22\sigma$
CMB + Lensing + Pantheon	$70.88 \pm 1.94$	$1.22\sigma$	$1.10\sigma$
CMB + All Data (BAO, CC, Pantheon, Lensing)	$70.18 \pm 1.79$	$1.51\sigma$	$1.44\sigma$

Table V: Tension between different  $H_0$  measurements with the values from Planck 2018 and R22 for the Perturbed  $f(R)$  gravity model.

Table VI: Cosmological Parameter Results for Different Datasets for perturbed  $f(R)$  gravity coupled with neutrinos

Parameter	CMB+Pantheon+Lensing	CMB+CC+Lensing	CMB+BAO+Lensing	CMB+Lensing	CMB+ALL
$\Omega_b h^2$	$0.02230 \pm 0.00022$	$0.02229 \pm 0.00024$	$0.02232 \pm 0.00021$	$0.02233 \pm 0.00023$	$0.02210 \pm 0.00016$
$\Omega_c h^2$	$0.1198 \pm 0.0036$	$0.1194 \pm 0.0039$	$0.1195 \pm 0.0033$	$0.1197 \pm 0.0034$	$0.1186 \pm 0.0022$
$100\theta_{MC}$	$1.0408 \pm 0.0006$	$1.0409 \pm 0.0007$	$1.0410 \pm 0.0005$	$1.04111 \pm 0.0006$	$1.0406 \pm 0.0004$
$\tau$	$0.058 \pm 0.008$	$0.059 \pm 0.009$	$0.0550 \pm 0.008$	$0.055 \pm 0.009$	$0.053^{+0.005}_{-0.007}$
$\ln(10^{10} A_s)$	$3.048 \pm 0.019$	$3.044 \pm 0.018$	$3.045 \pm 0.017$	$3.045 \pm 0.017$	$3.041^{+0.015}_{-0.016}$
$n_s$	$0.973 \pm 0.009$	$0.971 \pm 0.010$	$0.972 \pm 0.008$	$0.966 \pm 0.009$	$0.968 \pm 0.006$

suggests that Pantheon data contribute more towards aligning the results with late-time measurements compared to early-Universe constraints.

Finally, when all datasets (CMB, BAO, CC, Pantheon, and lensing) are combined, we obtain  $H_0 = 70.18 \pm 1.79$  km/s/Mpc, corresponding to tensions of  $1.51\sigma$  with Planck and  $1.44\sigma$  with R22. These results are broadly consistent with previous findings [98–101]. This comprehensive dataset combination slightly increases the overall tension compared to subsets but provides an intermediate  $H_0$  value between early and late Universe estimates.

In summary, none of the dataset combinations fully resolve the Hubble tension, though those incorporating Pantheon and CC data exhibit better agreement with local  $H_0$  measurements. The tension with Planck 2018 remains more significant, suggesting that while modified gravity models such as perturbed  $f(R)$  gravity shift the inferred  $H_0$  values, they do not entirely bridge the gap between early- and late-time Hubble constant determinations. Figure 2 illustrates the correlation between  $\Omega_m$  and  $H_0$  across different dataset combinations, while Figure 3 presents a visual representation of the cosmological parameters summarized in Table VII.

### Hubble Tension in Perturbed $f(R)$ Gravity Coupled with Neutrinos

In this section, we investigate the tension in the Hubble constant ( $H_0$ ) within the framework of perturbed  $f(R)$  gravity coupled with neutrinos, using a variety of cosmological datasets. The values of  $H_0$  obtained from different dataset combinations are compared against the Planck 2018 measurement ( $H_0^{\text{Planck 2018}} = 67.4 \pm 0.5$  km/s/Mpc) and the local SH0ES collaboration measurement, R22 ( $H_0^{\text{R22}} = 73.5 \pm 1.04$  km/s/Mpc).

The results are summarized in Table VIII, showing varying levels of tension with both Planck 2018 and R22. For the CMB and lensing data alone, we find a tension of  $0.74\sigma$  with Planck 2018 and  $0.95\sigma$  with R22. Adding BAO data increases the tension with Planck to  $1.14\sigma$ , while slightly increasing the tension with R22 to  $1.03\sigma$ .

When cosmic chronometer (CC) data is included alongside CMB and lensing, the inferred value  $H_0 = 70.26 \pm 2.38$  km/s/Mpc leads to a  $1.13\sigma$  tension with Planck and a  $0.98\sigma$  tension with R22, indicating a moderate shift towards the local measurement.

The combination of Pantheon (supernovae) data with CMB and lensing slightly reduces the tension with R22 to  $0.88\sigma$ , while increasing the tension with Planck 2018 to  $1.17\sigma$ .

Finally, incorporating all datasets—CMB, BAO, CC, Pantheon, and lensing—yields  $H_0 = 70.46 \pm 2.01$  km/s/Mpc, showing the highest level of tension with both Planck ( $1.42\sigma$ ) and R22 ( $1.12\sigma$ ).

Table VIII presents the full results. Figure 4 illustrates the correlation between  $\Omega_m$  and  $H_0$  for different dataset combinations, while Figure 5 demonstrates the cosmological parameter constraints for perturbed  $f(R)$  gravity coupled with neutrinos. These results are broadly consistent with previous findings [98–101].

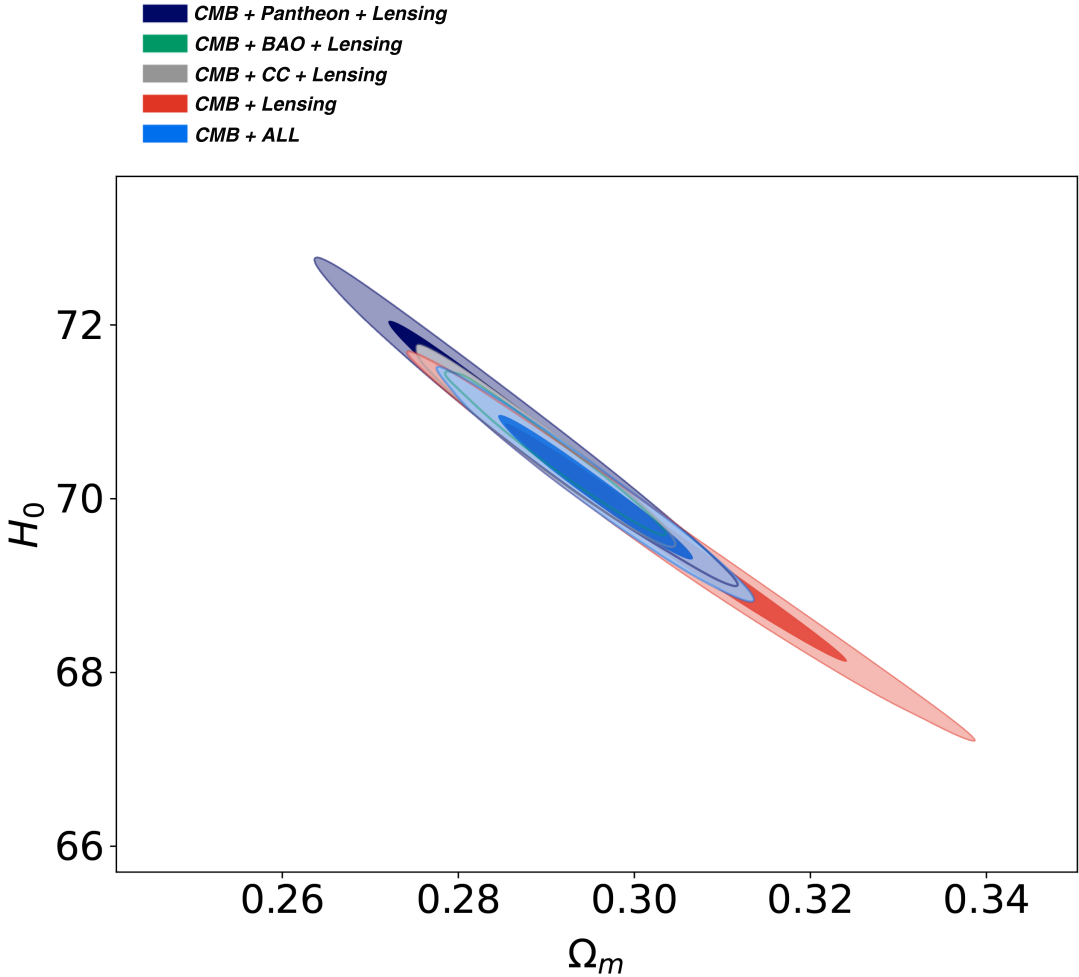


Figure 2: The comparison of  $\Omega_m$  vs  $H_0$  measurement for different combination of data sets(CMB+Other)for perturbed  $f(R)$  gravity model.

Dataset Combination	$H_0$ (km/s/Mpc)	Tension with Planck 2018	Tension with R22
CMB + Lensing	$69.82 \pm 3.12$	$0.74\sigma$	$0.95\sigma$
CMB + BAO + Lensing	$70.37 \pm 2.32$	$1.14\sigma$	$1.03\sigma$
CMB + Lensing + CC	$70.26 \pm 2.38$	$1.13\sigma$	$0.98\sigma$
CMB + Lensing + Pantheon	$70.57 \pm 2.54$	$1.17\sigma$	$0.88\sigma$
CMB + All Data (BAO, CC, Pantheon, Lensing)	$70.46 \pm 2.01$	$1.42\sigma$	$1.12\sigma$

Table VII: Tension between the Hubble constant derived from different dataset combinations and the values from Planck 2018 and R22 for the perturbed  $f(R)$  gravity model coupled with neutrinos.

#### $S_8$ Tension with Planck 2018, KiDS, and DES for Perturbed $f(R)$ Gravity

The parameter  $S_8$ , which combines the matter density  $\Omega_m$  and the amplitude of matter fluctuations  $\sigma_8$ , plays a crucial role in understanding the large-scale structure of the Universe. In our analysis, we find the  $S_8$  value for the CMB + All datasets to be  $S_8 = 0.798 \pm 0.030$ .

This result is slightly lower than the value inferred from the Planck CMB measurement, which gives  $S_8 = 0.832 \pm$

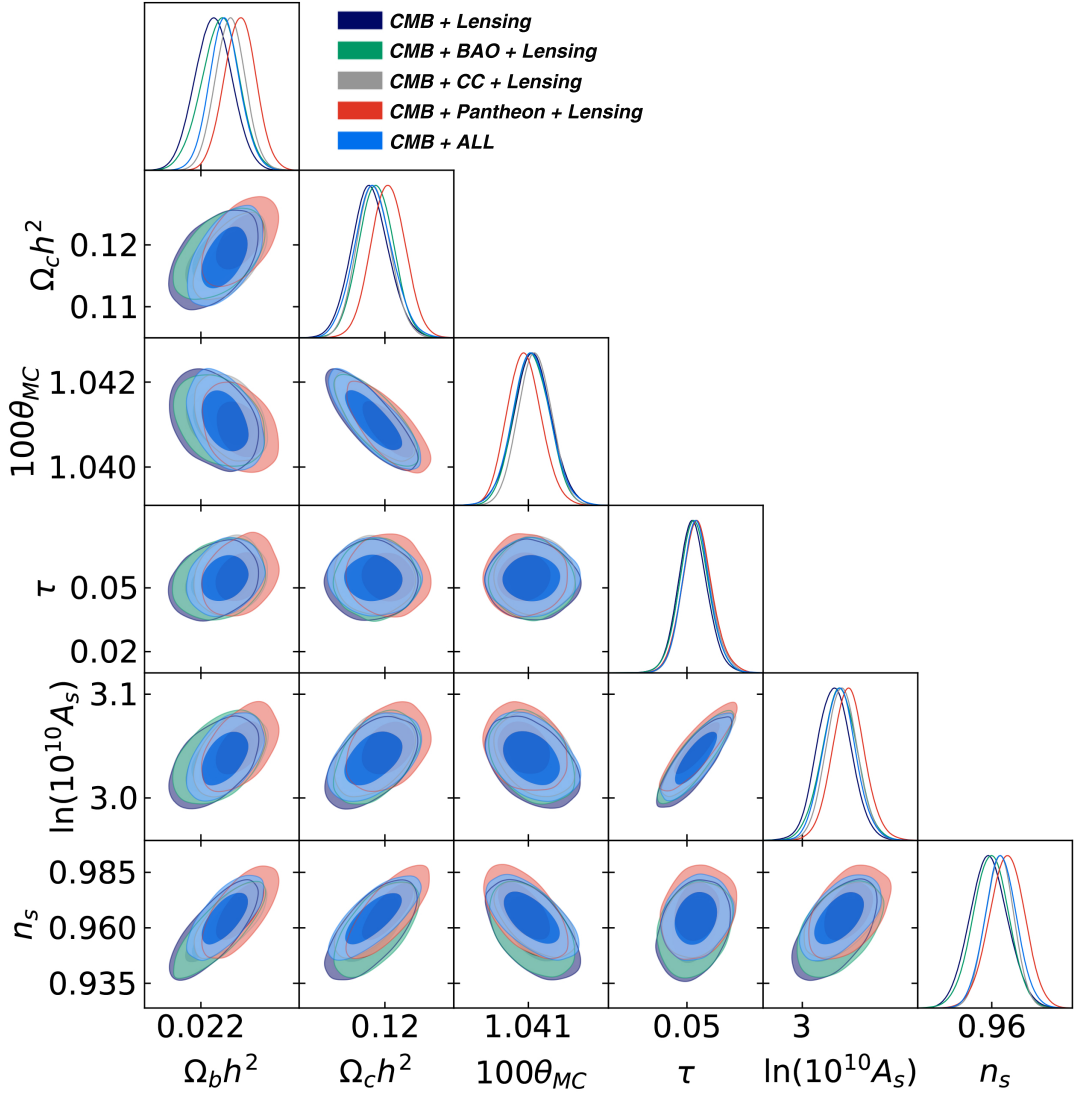


Figure 3: The comparison of cosmological parameters for different combination of data sets(CMB+Other) for perturbed  $f(R)$  gravity model.

Dataset	Value	Planck Tension	KiDS-1000 Tension	DES-Y3 Tension
CMB + Lensing	$S_8 = 0.808 \pm 0.066$	$0.53\sigma$	$0.49\sigma$	$0.68\sigma$
CMB + Lensing + BAO	$S_8 = 0.8 \pm 0.046$	$0.87\sigma$	$0.96\sigma$	$1.15\sigma$
CMB + Lensing + CC	$S_8 = 0.801 \pm 0.030$	$1.47\sigma$	$1.57\sigma$	$1.89\sigma$
CMB + Lensing + Pantheon	$S_8 = 0.802 \pm 0.048$	$0.79\sigma$	$0.81\sigma$	$1.02\sigma$
CMB + All	$S_8 = 0.798 \pm 0.030$	$1.43\sigma$	$1.15\sigma$	$1.32\sigma$

Table VIII: Summary of  $S_8$  tensions with Planck 2018, KiDS, and DES for the perturbed  $f(R)$  gravity model.

0.013 [82], indicating a moderate tension of approximately  $1.43\sigma$ .

Furthermore, when compared to measurements from KiDS-1000x{2dFLenS+BOSS}, which reports  $S_8 = 0.766^{+0.020}_{-0.014}$  [21], and DES-Y3, which provides  $S_8 = 0.776 \pm 0.017$  [22], the tension with our CMB + All result is about  $1.15\sigma$  and  $1.32\sigma$ , respectively.

These results underscore the ongoing challenge of reconciling cosmic microwave background data with large-scale structure observations within the framework of perturbed  $f(R)$  gravity, highlighting potential discrepancies between theoretical predictions and observational data. All the above results are summarized in Table VIII.

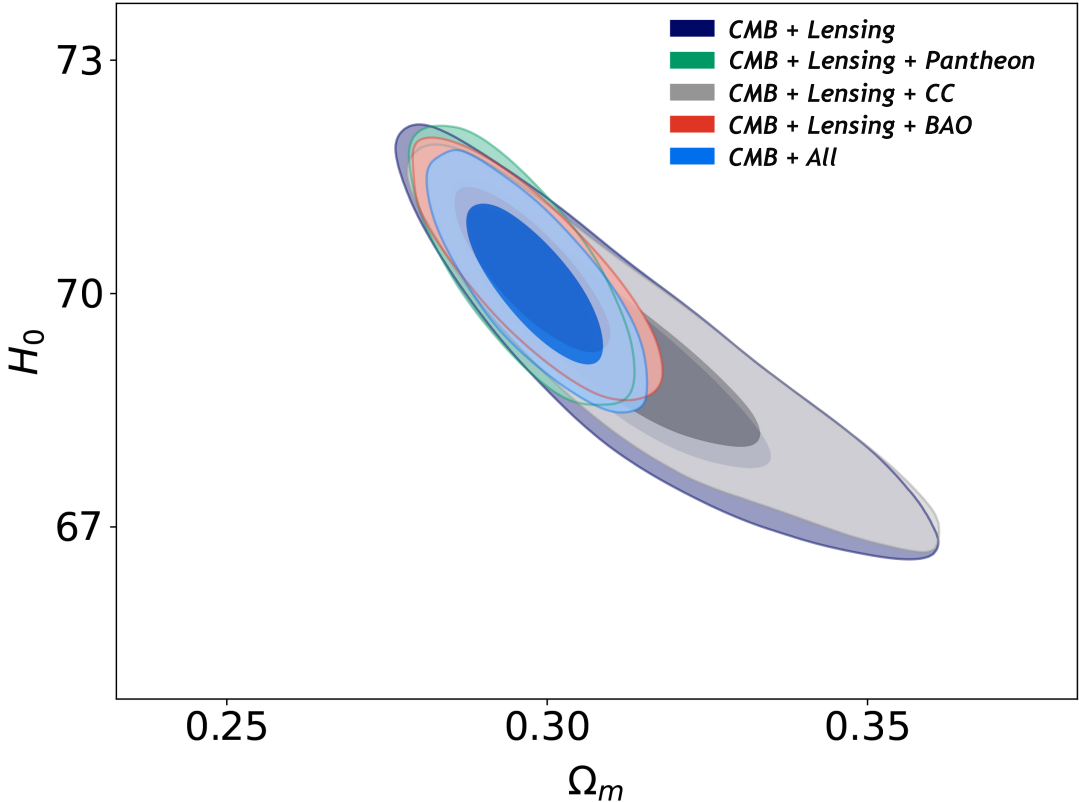


Figure 4: The comparison of  $\Omega_m$  vs  $H_0$  measurement for different combination of data sets(CMB+Other) perturbed  $f(R)$  gravity model coupled with neutrinos.

#### $S_8$ Tension with Planck 2018, KiDS, and DES for Perturbed $f(R)$ Gravity Coupled with Neutrinos

In our analysis within the framework of perturbed  $f(R)$  gravity coupled with neutrinos, we have derived  $S_8$  values from various combinations of observational datasets. A detailed summary of these results is presented in Table IX.

We find that the  $S_8$  value for the CMB + All datasets is  $S_8 = 0.785 \pm 0.046$ . When compared to the Planck 2018 result of  $S_8 = 0.832 \pm 0.013$  [82], this corresponds to a tension of approximately  $1.13\sigma$ . This moderate discrepancy suggests a possible deviation from the standard cosmological model.

Comparisons with large-scale structure surveys reveal further tensions. The KiDS-1000x{2dFLenS+BOSS} result of  $S_8 = 0.766^{+0.02}_{-0.014}$  [21] shows a tension of approximately  $0.70\sigma$  with our findings, while the DES-Y3 value of  $S_8 = 0.776 \pm 0.017$  [22] indicates a tension of around  $0.23\sigma$ .

These results highlight the challenges in reconciling cosmic microwave background data with large-scale structure observations within the perturbed  $f(R)$  gravity framework. The inclusion of neutrino coupling appears to reduce the level of tension with Planck and large-scale structure datasets compared to the standard cosmological model, suggesting that modified gravity and neutrino interactions may play a role in resolving the  $S_8$  tension.

The results show that the level of tension with the Planck 2018 results remains significant but is somewhat reduced

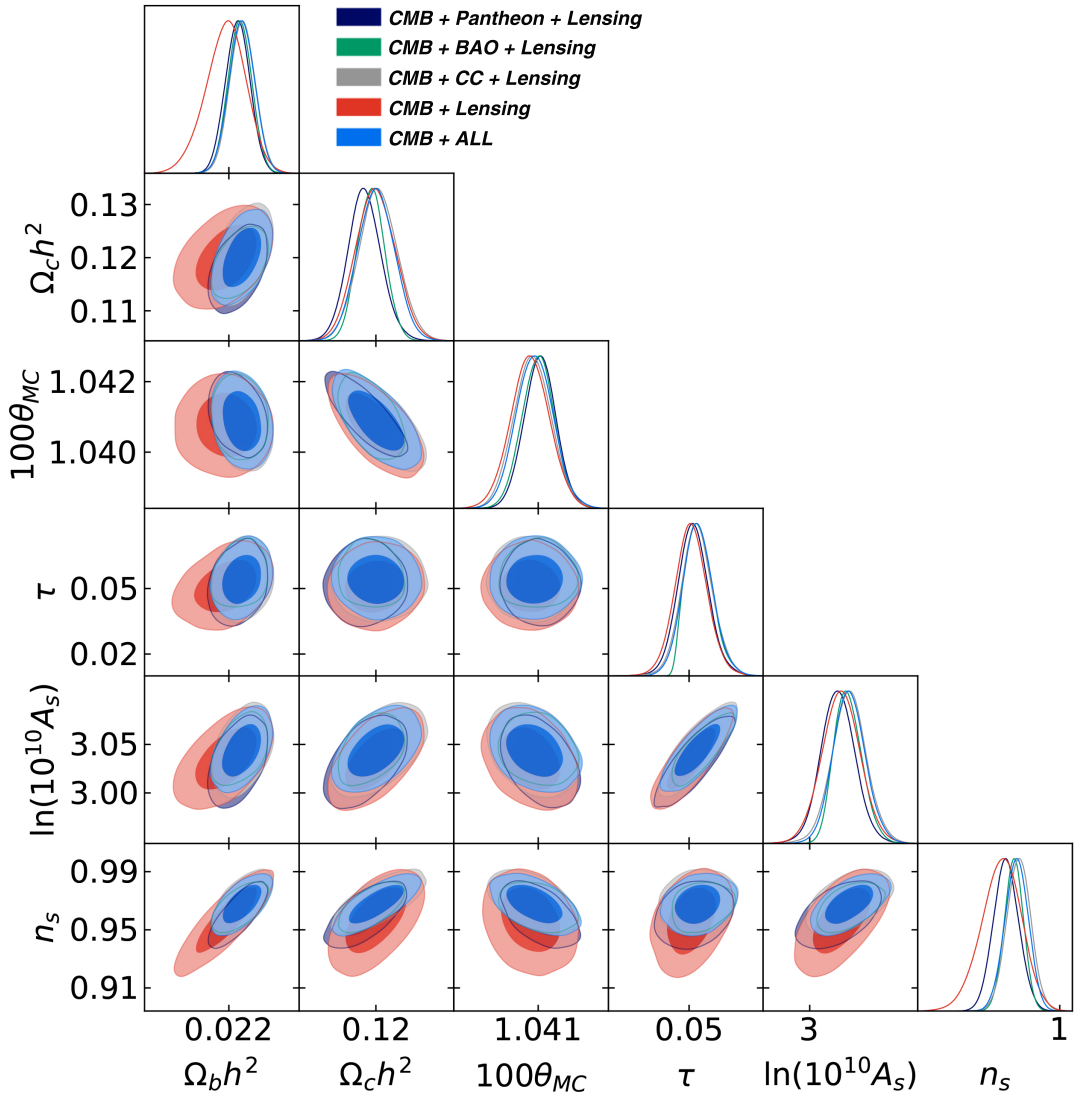


Figure 5: The comparison of cosmological parameters for different combination of data sets(CMB+Other) for perturbed  $f(R)$  gravity model coupled with neutrinos.

Dataset	Value	Tension with Planck	Tension with KiDS-1000	Tension with DES-Y3
CMB + Lensing	$S_8 = 0.784 \pm 0.065$	$0.74\sigma$	$0.86\sigma$	$0.46\sigma$
CMB + Lensing + BAO	$S_8 = 0.791 \pm 0.045$	$1.13\sigma$	$0.75\sigma$	$0.34\sigma$
CMB + Lensing + CC	$S_8 = 0.793 \pm 0.046$	$1.06\sigma$	$0.79\sigma$	$0.39\sigma$
CMB + Lensing + Pantheon	$S_8 = 0.792 \pm 0.058$	$0.86\sigma$	$0.72\sigma$	$0.36\sigma$
CMB + All	$S_8 = 0.785 \pm 0.046$	$1.13\sigma$	$0.70\sigma$	$0.23\sigma$

Table IX: Summary of  $S_8$  tensions with Planck 2018, KiDS-1000, and DES-Y3 for the perturbed  $f(R)$  gravity model coupled with neutrinos.

when compared to the standard cosmological model. Interestingly, the tensions with KiDS-1000 and DES-Y3 are relatively low, suggesting that the perturbed  $f(R)$  gravity model with neutrino coupling may provide a better fit to large-scale structure data.

Figures 6 and 7 present a comparison of the clustering amplitude parameter  $S_8$  for different combinations of data sets, including the cosmic microwave background (CMB) and other observational probes, within the context of perturbed  $f(R)$  gravity models. Figure 6 shows the results for the perturbed  $f(R)$  gravity model coupled without

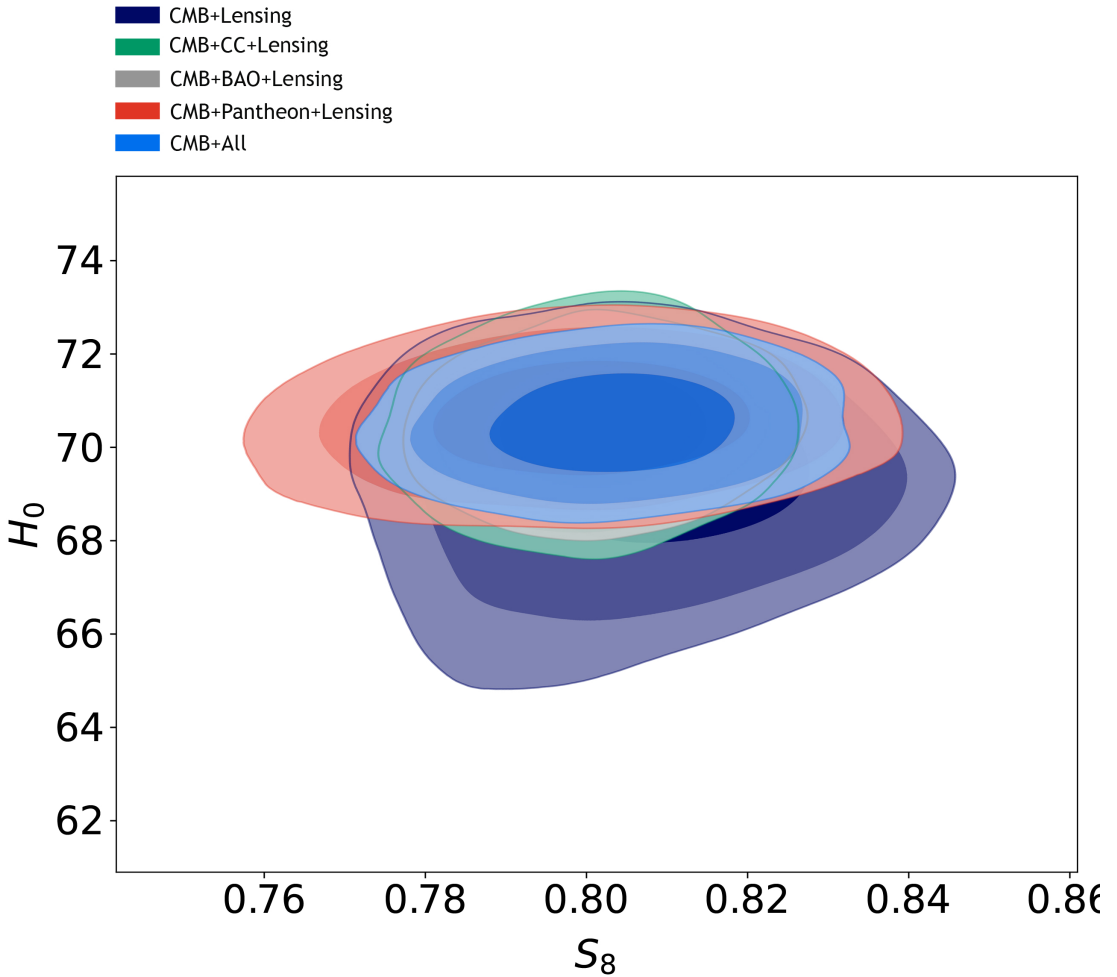


Figure 6: The comparison of  $S_8$  for different combination of data sets(CMB+Other) for perturbed  $f(R)$  gravity model.

neutrinos, highlighting the impact of neutrino coupling on the clustering amplitude. In contrast, Figure 7 illustrates the comparison for the perturbed  $f(R)$  gravity model with neutrino coupling, providing insight into the effects of modified gravity alone on the  $S_8$  parameter. These figures underscore the role of neutrino interactions and modified gravity in resolving the observed tension in the clustering amplitude.

## IX. CONCLUSION

This study investigated the Hubble constant ( $H_0$ ) in the context of the perturbed  $f(R)$  gravity model and its coupling with neutrinos, focusing on the discrepancies between early and late Universe measurements. By analyzing various combinations of observational datasets, including cosmic microwave background (CMB), baryon acoustic oscillations (BAO), cosmic chronometers (CC), Pantheon supernovae data, and lensing, we evaluated the extent to which these models could alleviate the Hubble tension.

For the perturbed  $f(R)$  gravity model, the inclusion of various datasets demonstrated a range of inferred  $H_0$  values, with tensions varying between  $0.61\sigma$  and  $1.51\sigma$  relative to Planck 2018 and between  $1.10\sigma$  and  $1.44\sigma$  relative to R22. While this model showed moderate improvements in the inferred  $H_0$  values, the tension with both early- and

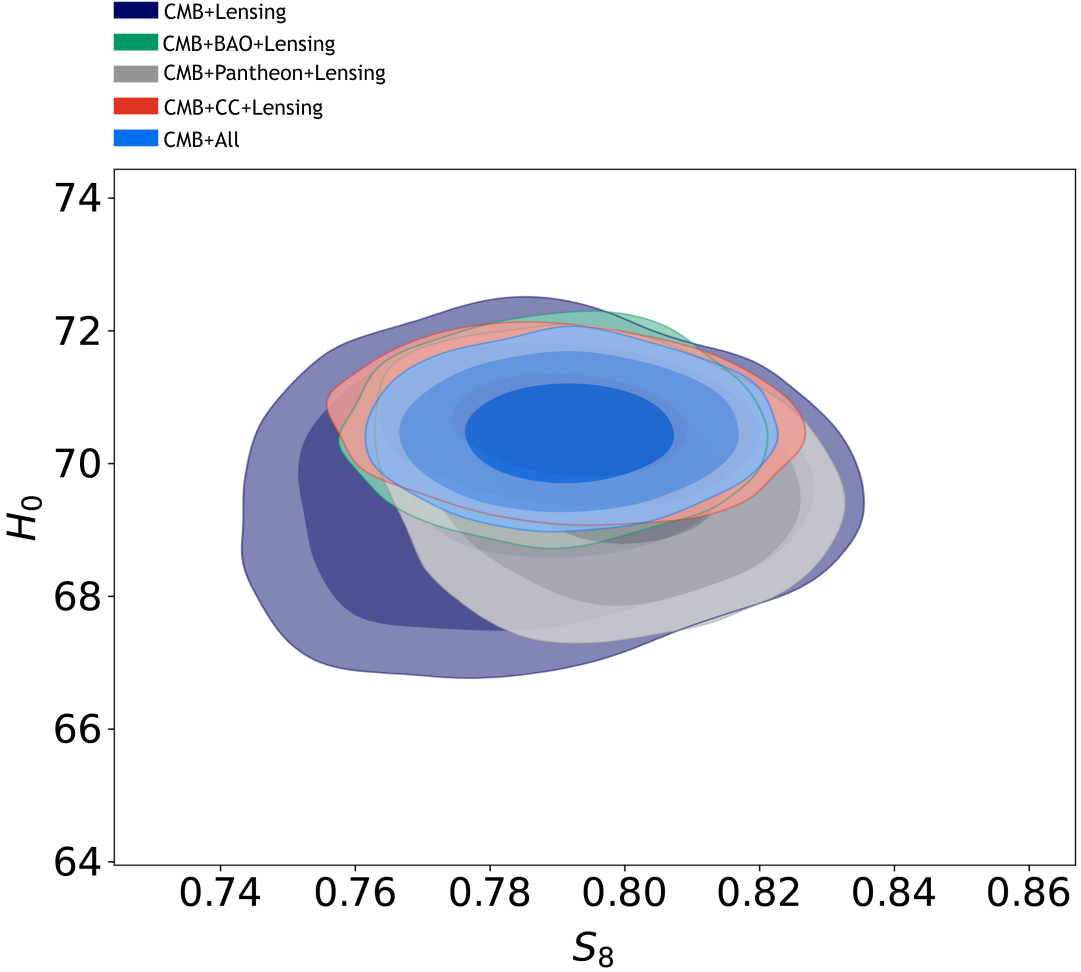


Figure 7: The comparison of  $S_8$  for different combination of data sets(CMB+Other) for perturbed  $f(R)$  gravity model coupled with neutrinos.

late-Universe measurements persisted, particularly when combining CMB data with other late-time probes.

In contrast, the perturbed  $f(R)$  gravity model coupled with neutrinos demonstrated a more significant potential to alleviate the Hubble tension. By incorporating the neutrino coupling, the inferred  $H_0$  values shifted closer to those from local measurements, reducing the tension more effectively than the non-coupled case. For certain combinations of datasets, the tension with Planck 2018 decreased to  $0.74\sigma$ , while the tension with R22 dropped to  $0.95\sigma$ , highlighting the promise of this extended model. The improved performance of the neutrino-coupled model underscores its capability to address the observed discrepancies between early- and late-time cosmological measurements. Our analysis of the parameter  $S_8$ , which combines the matter density  $\Omega_m$  and the amplitude of matter fluctuations  $\sigma_8$ , reveals moderate tension between the values inferred from cosmic microwave background (CMB) data and large-scale structure surveys within the framework of perturbed  $f(R)$  gravity models, both with and without neutrino coupling. For the non-interacting case, the  $S_8$  value for the CMB + All dataset is  $S_8 = 0.798 \pm 0.030$ , showing a  $1.43\sigma$  tension with Planck 2018 and tensions of approximately  $1.15\sigma$  and  $1.32\sigma$  with KiDS-1000 and DES-Y3, respectively. For the interacting case with neutrino coupling, the CMB + All result is  $S_8 = 0.785 \pm 0.046$ , reducing the tension with Planck to  $1.13\sigma$  and lowering the tensions with KiDS-1000 and DES-Y3 to  $0.70\sigma$  and  $0.23\sigma$ , respectively. These findings suggest that modified gravity and neutrino interactions may help mitigate the  $S_8$  tension and improve consistency.

with large-scale structure data. These results suggest that the perturbed  $f(R)$  gravity model, particularly when coupled with neutrinos, represents a promising framework for mitigating the Hubble and  $S_8$  tension. While it does not completely resolve the discrepancy, the improved agreement with late-time measurements indicates the potential of this model to account for deviations in cosmological observations. Future work should focus on further refining this framework, including exploring additional coupling mechanisms, quantum corrections, and interactions with dark energy, to better address the unresolved tensions.

In summary, the perturbed  $f(R)$  gravity model coupled with neutrinos offers a more effective approach to alleviating the Hubble and  $S_8$  tension compared to its non-coupled counterpart. This advancement paves the way for further theoretical and observational efforts to unravel the complexities of the Universe's expansion history.

---

[1] Planck Collaboration, P. A. R. Ade et al. *Astron. Astrophys.* **571** (2014) A16, arXiv:1303.5076.

[2] Planck Collaboration, P. A. R. Ade et al. *Astron. Astrophys.* **594** (2016) A13, arXiv:1502.01589.

[3] Planck Collaboration, N. Aghanim et al. *Planck 2018 results. VI. Cosmological parameters.* arXiv:1807.06209.

[4] A. G. Riess, S. Casertano, W. Yuan et al., *Astrophys J.* **861** (2018) 126, arXiv: 1804.10655.

[5] A. G. Riess, S. Casertano, W. Yuan, L. M. Macri and D. Scolnic, *Astrophys J.* **876** (2019) 85, arXiv: 1903.07603.

[6] L. Verde, T. Treu and A. G. Riess, *Nature Astronomy* **3** (2019) 891, arXiv:1907.10625.

[7] W. L. Freedman, B. F. Madore, D. Hatt et al., *Astrophys J.* **882** (2019) 34, arXiv:1907.05922.

[8] W. L. Freedman B. F. Madore, T. Hoyt et al., arXiv:2002.01550.

[9] K. C. Wong, S. H. Suyu, G. C.-F. Chen et al., 2019, *Mon. Not. Roy. Astron. Soc.*, doi:10.1093/mnras/stz3094, arXiv:1907.04869.

[10] J.-J. Wei and F. Melia, *Astrophys.J.* **897** (2020) 2, 127, arXiv:2005.10422.

[11] P. Denzel, J. P. Coles, P. Saha and L. L. R. Williams, The Hubble constant from eight time-delay galaxy lenses, arXiv:2007.14398.

[12] E. J. Baxter and B. D. Sherwin, arXiv:2007.04007.

[13] C. D. Huang, A. G. Riess, W. Yuan et al., 2019, *Astrophys. J.* **889** (2020) 1, 5, arXiv:1908.10883.

[14] Bergmann, Peter G. 1968. “Comments on the Scalar-Tensor Theory.” *International Journal of Theoretical Physics* **1**(1):25–36. doi: 10.1007/BF00668828.

[15] De Felice, Antonio, and Shinji Tsujikawa. 2010. “F(R) Theories.”

[16] Liu, Haishan, H. Lü, and Zhao-Long Wang. 2012. “F(R) Gravities, Killing Spinor Equations, ‘BPS’ Domain Walls and Cosmology.” *Journal of High Energy Physics* **2012**(2):83. doi: 10.1007/JHEP02(2012)083.

[17] Buchdahl, H. A. 1970. “Non-Linear Lagrangians and Cosmological Theory.” *Monthly Notices of the Royal Astronomical Society* **150**(1):1–8. doi: 10.1093/mnras/150.1.1.

[18] Oppenheimer, J. R., and H. Snyder. 1939. “On Continued Gravitational Contraction.” *Physical Review* **56**(5):455–59. doi: 10.1103/PhysRev.56.455.

[19] Darabi, F., K. Atazadeh, and Y. Heydarzade. 2017. “Einstein Static Universe in Rastall Theory of Gravity.”

[20] Fabris, J. C., M. Hamani Daouda, and O. F. Piattella. 2012. “Note on the Evolution of the Gravitational Potential in Rastall Scalar Field Theories.” *Physics Letters B* **711**(3–4):232–37. doi: 10.1016/j.physletb.2012.04.020.

[21] T. M. C. Abbott et al. (DES, SPT), “Joint analysis of DES Year 3 data and CMB lensing from SPT and Planck III: Combined cosmological constraints,” (2022), arXiv:2206.10824 [astro-ph.CO].

[22] Catherine Heymans et al., “KiDS-1000 Cosmology: Multi-probe weak gravitational lensing and spectroscopic galaxy clustering constraints,” *Astron. Astrophys.* **646**, A140 (2021), arXiv:2007.15632 [astro-ph.CO].

[23] P. Rastall, *Phys. Rev.* **D6**, 3357 (1972).

[24] Y. Heydarzade and F. Darabi, *Phys. Lett.* **B771**, 365 (2017), arXiv:1702.07766.

[25] J. P. Moraes Graca and I. P. Lobo, *Eur. Phys. J.* **C78**, 101 (2018), arXiv:1711.08714.

[26] K. A. Bronnikov, J. C. Fabris, O. F. Piattella, and E. C. Santos, *Gen. Rel. Grav.* **48**, 162 (2016), arXiv:1606.06242.

[27] Y. Heydarzade, H. Moradpour, and F. Darabi, *Can. J. Phys.* **95**, 1253 (2017), arXiv:1610.03881.

[28] E. Spallucci and A. Smailagic, *Int. J. Mod. Phys.* **D27**, 1850003 (2017), arXiv:1709.05795.

[29] R. Kumar and S. G. Ghosh, *Eur. Phys. J.* **C78**, 750 (2018), arXiv:1711.08256.

[30] Z. Xu, X. Hou, X. Gong, and J. Wang, *Eur. Phys. J.* **C78**, 513 (2018), arXiv:1711.04542.

[31] M. Sadeghi, (2018), arXiv:1809.08698.

[32] I. P. Lobo, H. Moradpour, J. P. Moraes Gracurca, and I. G. Salako, *Int. J. Mod. Phys.* **D27**, 1850069 (2018), arXiv:1710.04612.

[33] K. Lin, Y. Liu, and W.-L. Qian, *Gen. Rel. Grav.* **51**, 62 (2019), arXiv:1809.10075.

[34] K. Lin and W.-L. Qian, *Chin. Phys.* **C43**, 083106 (2019), arXiv:1812.10100.

[35] A. S. Al-Rawaf and M. O. Taha, *Phys. Lett.* **B366**, 69 (1996).

[36] A. S. Al-Rawaf and M. O. Taha, *Gen. Rel. Grav.* **28**, 935 (1996).

[37] C. E. M. Batista, M. H. Daouda, J. C. Fabris, O. F. Piattella, and D. C. Rodrigues, *Phys. Rev.* **D85**, 084008 (2012),

arXiv:1112.4141.

[38] J. C. Fabris, O. F. Piattella, D. C. Rodrigues, C. E. M. Batista, and M. H. Daouda, Int. J. Mod. Phys. Conf. Ser. **18**, 67 (2012), arXiv:1205.1198.

[39] K. A. Bronnikov, J. C. Fabris, O. F. Piattella, D. C. Rodrigues, and E. C. Santos, Eur. Phys. J. **C77**, 409 (2017), arXiv:1701.06662.

[40] F. Darabi, K. Atazadeh, and Y. Heydarzadeh, Eur. Phys. J. Plus **133**, 249 (2018), arXiv:1710.10429.

[41] F.-F. Yuan and P. Huang, Class. Quant. Grav. **34**, 077001 (2017), arXiv:1607.04383.

[42] J. C. Fabris, M. H. Daouda, and O. F. Piattella, Phys. Lett. **B711**, 232 (2012), arXiv:1109.2096.

[43] C. E. M. Batista, J. C. Fabris, O. F. Piattella, and A. M. Velasquez-Toribio, Eur. Phys. J. **C73**, 2425 (2013), arXiv:1208.6327.

[44] H. Moradpour, Y. Heydarzadeh, F. Darabi, and I. G. Salako, Eur. Phys. J. **C77**, 259 (2017), arXiv:1704.02458.

[45] S. Weinberg, Rev. Mod. Phys. **61**, 1 (1989), [569(1988)].

[46] T. Padmanabhan, Phys. Rept. **380**, 235 (2003), arXiv:hep-th/0212290.

[47] E. J. Copeland, M. Sami, and S. Tsujikawa, Int. J. Mod. Phys. **D15**, 1753 (2006), arXiv:hep-th/0603057.

[48] K. Bamba, S. Capozziello, S. Nojiri, and S. D. Odintsov, Astrophys. Space Sci. **342**, 155 (2012), arXiv:1205.3421.

[49] M. Li, X.-D. Li, S. Wang, and Y. Wang, Commun. Theor. Phys. **56**, 525 (2011), arXiv:1103.5870.

[50] R. R. Caldwell, R. Dave, and P. J. Steinhardt, Phys. Rev. Lett. **80**, 1582 (1998), arXiv:astro-ph/9708069.

[51] A. Sen, JHEP **07**, 065 (2002), arXiv:hep-th/0203265.

[52] C. Armendariz-Picon, V. F. Mukhanov, and P. J. Steinhardt, Phys. Rev. Lett. **85**, 4438 (2000), arXiv:astro-ph/0004134.

[53] S. Nojiri and S. D. Odintsov, Phys. Lett. **B562**, 147 (2003), arXiv:hep-th/0303117.

[54] A. Yu. Kamenshchik, U. Moschella, and V. Pasquier, Phys. Lett. **B511**, 265 (2001), arXiv:gr-qc/0103004.

[55] A. G. Cohen, D. B. Kaplan, and A. E. Nelson, Phys. Rev. Lett. **82**, 4971 (1999), arXiv:hep-th/9803132.

[56] M. Li, Phys. Lett. **B603**, 1 (2004), arXiv:hep-th/0403127.

[57] B. Wang, Y.-g. Gong, and E. Abdalla, Phys. Lett. **B624**, 141 (2005), arXiv:hep-th/0506069.

[58] R.-G. Cai, Phys. Lett. **B657**, 228 (2007), arXiv:0707.4049.

[59] H. Wei and R.-G. Cai, Phys. Lett. **B660**, 113 (2008), arXiv:0708.0884.

[60] A. De Felice and S. Tsujikawa, Living Rev. Rel. **13**, 3 (2010), arXiv:1002.4928.

[61] F. W. Hehl, J. D. McCrea, E. W. Mielke, and Y. Ne’eman, Phys. Rept. **258**, 1 (1995), arXiv:gr-qc/9402012.

[62] T. Harko, F. S. N. Lobo, S. Nojiri, and S. D. Odintsov, Phys. Rev. **D84**, 024020 (2011), arXiv:1104.2669.

[63] C. Brans and R. H. Dicke, Phys. Rev. **124**, 925 (1961), [142(1961)].

[64] S. Nojiri and S. D. Odintsov, Phys. Lett. **B631**, 1 (2005), arXiv:hep-th/0508049.

[65] D. Lovelock, J. Math. Phys. **12**, 498 (1971).

[66] P. Horava, Phys. Rev. **D79**, 084008 (2009), arXiv:0901.3775.

[67] P. Horava, Phys. Rev. Lett. **102**, 161301 (2009), arXiv:0902.3657.

[68] K. Lin, A. Wang, Q. Wu, and T. Zhu, Phys. Rev. **D84**, 044051 (2011), arXiv:1106.1486.

[69] K. Lin, S. Mukohyama, A. Wang, and T. Zhu, Phys. Rev. **D89**, 084022 (2014), arXiv:1310.6666.

[70] Capozziello S. and De Laurentis M.,(2011), Phys. Rept. 509 , 167-321 [arXiv:1108.6266 [gr-qc]].

[71] Capozziello S.,(2002), Int. J. Mod. Phys. D 11 , 483-492 [arXiv:gr-qc/0201033 [gr-qc]].

[72] Capozziello S. and Francaviglia M.,(2008) , Gen. Rel. Grav. 40 357-420, arXiv:0706.1146 [astro-ph]. 3, 16, 39, 50

[73] De Felice A. and Tsujikawa S.,(2010), Living Rev. Rel. 13 , 3 [arXiv:1002.4928 [gr-qc]].

[74] Nojiri S. and Odintsov S. D.,(2006), eConf C0602061 , 06 [arXiv:hep-th/0601213 [hep-th]].

[75] Nojiri S.i and Odintsov S. D.,(2003), Phys. Rev. D 68 , 123512 [arXiv:hep-th/0307288 [hep-th]].

[76] Sotiriou T. P. and Faraoni V.,(2010), Rev. Mod. Phys. 82 , 451-497 [arXiv:0805.1726 [gr-qc]].

[77] Phillips M. M., 1993, ApJ, 413, L105

[78] Scolnic, D. et al. ,(2022), ApJ, Volume 938, Number 2

[79] Shulei Cao, Bharat Ratra, Phys. Rev. D 107, 103521 (2023)

[80] N. Aghanim, et al., arXiv:1907.12875 , Planck Collaboration

[81] Aghanim, N. et al., arXiv:1907.12875 , Planck Collaboration

[82] Aghanim, N.; Akrami, Y.; Ashdown, M.; Aumont, J.; Baccigalupi, C.; Ballardini, M.; Banday, A.J.; Barreiro, R.; Bartolo, N.; Basak, S. Planck 2018 results-VIII. Gravitational lensing. Astron. Astrophys. 2020, 641, A8.

[83] Gelman, A. and Rubin, D. B.,1992, Statist. Sci. 7, 457–472 .

[84] Lewis, A. and Bridle, S.,2002, Phys. Rev. D 66, 103511 .

[85] Lewis, A.,2013, Phys. Rev. D 87, 103529 .

[86] Kai Lin, Wei-Liang Qian,Eur. Phys. J. C (2020) 80: 561 https://doi.org/10.1140/epjc/s10052-020-8116-2

[87] Suárez, Abril, and Pierre-Henri Chavanis. 2018. “Jeans Type Instability of a Complex Self-Interacting Scalar Field in General Relativity.” Physical Review D 98(8):083529. doi: 10.1103/PhysRevD.98.083529.

[88] Wali Hossain, Md. Myrzakulov, R. Sami, M. Saridakis, E. N.,(2014),Phys. Rev. D 90, 023512 (2014)

[89] M Yarahmadi, A Salehi. The European Physical Journal C 83 (910 (2023)).

[90] Cardona, W., & Sabogal, M.A., 2023, JCAP, 2023, 045

[91] Di Valentino E, Mukherjee A, Sen AA. , 2021; 23(4):404. https://doi.org/10.3390/e23040404

[92] De Felice, A., & Tsujikawa, S. (2010). f(R) Theories. *Living Reviews in Relativity*, 13(3). <https://doi.org/10.12942/lrr-2010-3>

[93] Kolb, E. W., & Turner, M. S. (1990). *The Early Universe*. Frontiers in Physics. Addison-Wesley Publishing Company. ISBN: 0201626748

[94] Sotiriou, T. P., & Faraoni, V. (2010). f(R) Theories of Gravity. *Reviews of Modern Physics*, 82(1), 451. <https://doi.org/10.1103/RevModPhys.82.451>

[95] Nojiri, S., & Odintsov, S. D. (2011). Unified cosmic history in modified gravity: from  $f(R)$  theory to Lorentz non-invariant models. *Physics Reports*, 505(2-4), 59-144. <https://doi.org/10.1016/j.physrep.2011.04.001>

[96] Lesgourgues, J., & Pastor, S. (2006). Massive neutrinos and cosmology. *Physics Reports*, 429(6), 307-379. <https://doi.org/10.1016/j.physrep.2006.04.001>

[97] Luisa G. Jaime, Leonardo Patino, Marcelo Salgado, 2012, <https://doi.org/10.48550/arXiv.1206.1642>

[98] M Yarahmadi, A Salehi. 2024, MNRAS, Pages 3055–3067, <https://doi.org/10.1093/mnras/stae2257>.

[99] M Yarahmadi. 2024, Physics of dark universe. Volume 47, 101733, [https://doi.org/10.1016/j.dark.2024.101733..](https://doi.org/10.1016/j.dark.2024.101733)

[100] M Yarahmadi. 2024, <https://doi.org/10.1140/epjc/s10052-024-12805-7>

[101] M. Yarahmadi et al. ,2025,physics of dark universe, <https://doi.org/10.1016/j.dark.2025.101824>

[102] A. Salehi et al. ,2020,EPJC, Volume 80, article number 753, (2020)

[103] P. Carter, F. Beutler, W. J. Percival, C. Blake, J. Koda, and A. J. Ross, “Low redshift baryon acoustic oscillation measurement from the reconstructed 6-degree field galaxy survey,” *Mon. Not. R. Astron. Soc.*, vol. 481, p. 2371, 2018, arXiv:1803.01746 [astro-ph.CO].

[104] H. Gil-Marín, J. E. Bautista, R. Paviot, M. Vargas-Magaña, S. de la Torre, S. Fromenteau, S. Alam, S. Ávila, E. Burtin, C.-H. Chuang, et al., “The Completed SDSS-IV extended Baryon Oscillation Spectroscopic Survey: measurement of the BAO and growth rate of structure of the luminous red galaxy sample from the anisotropic power spectrum between redshifts 0.6 and 1.0,” *Mon. Not. R. Astron. Soc.*, vol. 498, p. 2492, 2020, arXiv:2007.08994 [astro-ph.CO].

[105] J. E. Bautista, R. Paviot, M. Vargas Magaña, S. de la Torre, S. Fromenteau, H. Gil-Marín, A. J. Ross, E. Burtin, K. S. Dawson, J. Hou, et al., “The completed SDSS-IV extended Baryon Oscillation Spectroscopic Survey: measurement of the BAO and growth rate of structure of the luminous red galaxy sample from the anisotropic correlation function between redshifts 0.6 and 1,” *Mon. Not. R. Astron. Soc.*, vol. 500, p. 736, 2021, arXiv:2007.08993 [astro-ph.CO].

[106] DES Collaboration, “Dark Energy Survey Year 3 results: A 2.7% measurement of baryon acoustic oscillation distance scale at redshift 0.835,” *Phys. Rev. D*, vol. 105, p. 043512, 2022, arXiv:2107.04646 [astro-ph.CO].

[107] R. Neveux, E. Burtin, A. de Mattia, A. Smith, A. J. Ross, J. Hou, J. Bautista, J. Brinkmann, C.-H. Chuang, K. S. Dawson, et al., “The completed SDSS-IV extended Baryon Oscillation Spectroscopic Survey: BAO and RSD measurements from the anisotropic power spectrum of the quasar sample between redshift 0.8 and 2.2,” *Mon. Not. R. Astron. Soc.*, vol. 499, p. 210, 2020, arXiv:2007.08999 [astro-ph.CO].

[108] J. Hou, A. G. Sánchez, A. J. Ross, A. Smith, R. Neveux, J. Bautista, E. Burtin, C. Zhao, R. Scoccimarro, K. S. Dawson, et al., “The completed SDSS-IV extended Baryon Oscillation Spectroscopic Survey: BAO and RSD measurements from anisotropic clustering analysis of the quasar sample in configuration space between redshift 0.8 and 2.2,” *Mon. Not. R. Astron. Soc.*, vol. 500, p. 1201, 2021, arXiv:2007.08998 [astro-ph.CO].

[109] H. du Mas des Bourboux, J. Rich, A. Font-Ribera, V. de Sainte Agathe, J. Farr, T. Etourneau, J.-M. Le Goff, A. Cuceu, C. Balland, J. E. Bautista, et al., ‘The Completed SDSS-IV Extended Baryon Oscillation Spectroscopic Survey: Baryon Acoustic Oscillations with Ly $\alpha$  Forests,’ *Astrophys. J.*, vol. 901, p. 153, 2020, arXiv:2007.08995 [astro-ph.CO].

[110] Luisa G. Jaime, Leonardo Patino, Marcelo Salgado, 2012, <https://doi.org/10.48550/arXiv.1206.1642>

[111] B. Audren, J. Lesgourgues, K. Benabed, and S. Prunet, “Conservative Constraints on Early Cosmology with MontePython,” *JCAP*, vol. 2013, no. 02, p. 001, 2013,

[112] T. Brinckmann and J. Lesgourgues, “MontePython 3: Boosted MCMC sampler and other features,” *Phys. Dark Univ.*, vol. 24, p. 100260, 2019,

[113] D. Blas, J. Lesgourgues, and T. Tram, “The Cosmic Linear Anisotropy Solving System (CLASS). Part II: Approximation schemes,” *JCAP*, vol. 2011, no. 07, p. 034, 2011,

[114] Planck Collaboration, “Planck 2018 results. VI. Cosmological parameters,” *Astron. Astrophys.*, vol. 641, p. A6, 2020,

[115] D. M. Scolnic *et al.*, “The Complete Light-curve Sample of Spectroscopically Confirmed SNe Ia from Pan-STARRS1 and Cosmological Constraints from the Combined Pantheon Sample,” *Astrophys. J.*, vol. 859, no. 2, p. 101, 2018,